Journal of Controlled Release 384 (2025) 113850

Contents lists available at ScienceDirect

Journal of Controlled Release

journal homepage: www.elsevier.com/locate/jconrel

Amphiphilic dendrimer-assisted delivery of antisense nucleic acid mimics against *E. coli*☆

Mariana Gomes [a,b], Igor Resende [a,b], Yana Zamoshchak [a,b,c], Daniela Araújo [d,e], Joana Castro [d,e], Dinesh Dhumal [f], Ling Peng [f], Rita S. Santos [a,b], Nuno F. Azevedo [a,b,*]

[a] LEPABE - Laboratory for Process Engineering, Environment, Biotechnology and Energy, Faculty of Engineering, University of Porto, Rua Dr Roberto Frias, 4200-465 Porto, Portugal
[b] ALiCE - Associate Laboratory in Chemical Engineering, Faculty of Engineering, University of Porto, Rua Dr Roberto Frias, 4200-465 Porto, Portugal
[c] Faculty of Pharmaceutical, Biomedical and Veterinary Sciences, University of Antwerp, Antwerp, Belgium
[d] INIAV - National Institute for Agrarian and Veterinary Research, Rua dos Lagidos, Lugar da Madalena, Vairão, 4485-655 Vila do Conde, Portugal
[e] CEB - Centre of Biological Engineering, University of Minho, Campus of Gualtar, 4710-057 Braga, Portugal
[f] CINaM - Interdisciplinary Center of Nanoscience of Marseille, Aix-Marseille Université, CNRS UMR 7325, 13288 Marseille, France

ARTICLE INFO

Keywords:
Amphiphilic dendrimers
Locked nucleic acid
Peptide nucleic acid
Bacteria
Antinsense

ABSTRACT

The rise in antimicrobial resistance and the consequent ineffectiveness of conventional antibiotics emphasise the need for novel therapeutic strategies. Antisense nucleic acid mimics (NAMs) are emerging as promising precision therapeutic agents, inhibiting specific genes through hybridisation with selected nucleic acid targets. However, delivering NAMs into bacteria remains a significant challenge. This study explores the use of poly(amidoamine) (PAMAM) amphiphilic dendrimers (ADs) as delivery vehicles for NAMs targeting the essential *acpP* gene in *Escherichia coli*. Two ADs bearing primary amine or tertiary amine terminals, 1a and 1b, were tested for their ability to permeabilise the bacterial envelope, facilitate NAM internalisation, and enhance NAM-based antibacterial activity. Physicochemical characterisation studies, flow cytometry measurements, fluorescence and electron microscopy imaging, bacterial viability assays, and an in vivo toxicity assessment using a greater wax moth (*Galleria mellonella*) model were conducted. Both ADs acted as permeabilisers of the bacterial envelope and assisted in NAM internalisation and antibacterial activity. The most effective formulation, 1b combined with the peptide nucleic acid (PNA)-based NAM, achieved an 8 $\log_{10}$ reduction in viable bacteria, with sustained activity up to 24 h against *E. coli*. *In vivo*, the most promising formulations showed no toxicity, with *G. mellonella* larvae maintaining overall health and no significant mortality detected for up to three days. These findings demonstrate that amphiphilic dendrimers can effectively deliver PNA-based NAMs, highlighting their potential as a novel strategy against antimicrobial-resistant pathogens.

1. Introduction

Antimicrobial resistance (AMR) is among the most pressing public health challenges of our time, with current estimates indicating it will be associated with 8.22 million annual deaths globally by 2050 if alternatives to existing antibiotics are not developed [1–3]. Although *Escherichia coli* is a common and generally harmless member of the gut microbiota, its pathogenic strains have a predominant role in urinary tract infections, foodborne illnesses and bacteremia [4]. This Gram-negative bacterium is one of the ESKAPE pathogens (which groups *Enterococcus faecium*, *Staphylococcus aureus*, *Klebsiella pneumoniae*, *Acinetobacter baumannii*, *Pseudomonas aeruginosa*, and *Enterobacter* spp.) recognised for their high prevalence of AMR [5]. It has also been included in the latest World Health Organisation (WHO) priority pathogens list, due to its cephalosporin-resistant variants and clinical significance, having been responsible for almost 1 million deaths worldwide in 2019 [3,5–7]. Additionally, *E. coli* has been reported to easily acquire resistance genes through horizontal gene transfer [8], exacerbating the challenge of treating multidrug-resistant infections. Therefore, developing novel antibacterial compounds and strategies

☆ This article is part of a Special issue entitled: 'SPLC-CRS_2024_Conference' published in Journal of Controlled Release.

* Corresponding author at: LEPABE - Laboratory for Process Engineering, Environment, Biotechnology and Energy, Department of Chemical Engineering, Faculty of Engineering, University of Porto, Rua Dr Roberto Frias s/n, 4200-465 Porto, Portugal.
E-mail address: nazevedo@fe.up.pt (N.F. Azevedo).

https://doi.org/10.1016/j.jconrel.2025.113850
Received 27 November 2024; Received in revised form 24 April 2025; Accepted 14 May 2025
Available online 23 May 2025

against pathogenic *E. coli* is a critical priority.

Oligonucleotides based on nucleic acid mimics (NAMs) can become an alternative to traditional antibiotics due to their capability to target a selected coding messenger RNA (mRNA) and, via hybridisation and steric blocking, inhibit its translation in an effective and specific manner [9–12]. By inhibiting the expression of essential genes present in the bacterial cytosol, NAMs can ultimately lead to bacterial death. Several essential genes have been studied as possible targets [13], including the *acpP* gene, which encodes a protein involved in fatty acid biosynthesis, and is widely established as a target in antisense strategies in *E. coli* [13–15]. To increase biostability and promote interaction with the target, a variety of NAM chemistries have been developed. Among them, peptide nucleic acid (PNA) is one of the most extensively studied, providing a neutral pseudo-peptide backbone to the antisense sequence. The neutral scaffold minimises electrostatic repulsion in the resulting PNA:RNA hybrids, enhancing their stability and reducing sensitivity to salt concentrations, thereby broadening their functional range [16,17]. Alternatively, chemistries with modified ribose entities, such as 2'-O-methyl RNA (2'O-Me) or locked nucleic acid (LNA), carry a negatively charged phosphate backbone similar to that of RNA. 2'O-Me involves the addition of a methyl group at the 2' carbon of the ribose moiety and has gained popularity as it provides stability against nucleases. LNA presents a restricted conformation due to a methylene bridge connecting the 2′ oxygen and the 4′ carbon, and is known for its high binding affinity to the RNA targets. When combined, they allow the synthesis of a variety of NAMs which can be fine-tuned with regard to binding affinity and rigidity, optimising the NAM's hybridisation properties [18–20]. Unlike traditional antibiotics that often affect both harmful and beneficial bacteria, NAMs offer a high degree of specificity, minimising off-target effects and reducing the likelihood of resistance development [12,21]. However, the potential of NAMs has so far been hindered by their inability to cross the multi-layered bacterial envelopes [11,12]. While our group has shown that fusogenic liposomes are promising for NAM delivery across this barrier [22,23], recent work suggests that even higher delivery efficiencies are required to reliably treat infections [23,24].

Amphiphilic dendrimers (ADs), also known as lipid-dendrimer hybrids, are a family of synthetic amphiphiles characterised by their chimaeric nature. They are composed of a hydrophobic entity and a highly branched hydrophilic dendron that resembles the shape of a dendrite (a tree-like structure). They were originally inspired by both lipids and traditional dendrimers to capitalise on the advantages of both, such as self-assembly and multivalent cooperativity, while overcoming some of their limitations, such as the complex synthesis and associated toxicity [25–28]. Their amphiphilic nature allows for self-assembly into supramolecular nanomicelles which are expectedly smaller than liposomes [29–32]. Additionally, ADs can carry cationic groups, such as primary amines, tertiary amines or guanidines, due to their surface modification potential. These groups increase the overall positive charge and can potentiate electrostatic interaction with the negatively charged bacterial envelopes, in particular, the outer membrane of Gram-negative bacteria [32]. Some of these ADs have already been proposed for the delivery in eukaryotic cells of small interfering RNA (siRNA) for gene silencing [27,28,30,31,33–37] and, to a lesser degree, mRNA and DNA for gene modulation [28,37]. While multiple AD designs can be explored, those currently found in the literature have consistently shown successful complexation with nucleic acid molecules via electrostatic coupling alongside hydrophobic interactions. Besides having shown efficient siRNA delivery and effective gene silencing, they were accompanied by low toxicity and immunogenicity *in vivo* [27,28]. Beyond gene therapy, ADs have also been employed for the delivery of anticancer drugs [29,38,39], for bioimaging purposes [40–43], and as antibacterials [32,44,45]. However, there have been no reports on the use of ADs as carriers to deliver NAMs as therapeutics against pathogenic bacteria.

In this study, two amphiphilic dendrimers, 1a and 1b, were employed for the delivery of antisense NAMs in *E. coli* (Fig. 1). The selected ADs are composed of a long hydrophobic alkyl chain and a hydrophilic poly(amidoamine) (PAMAM) dendron, differing only in their terminal functionalities: while 1a carries primary amines as terminal groups, 1b bears tertiary amine terminals (Fig. 1A). Both ADs have been studied for their ability to efficiently deliver siRNA in mammalian cells [30,31,33] and were recently reported to have antibacterial activity [32,44,45]. Two NAM-based oligos, an LNA/2′O-Me chimaera and a PNA-based sequence, were selected for this proof of concept.

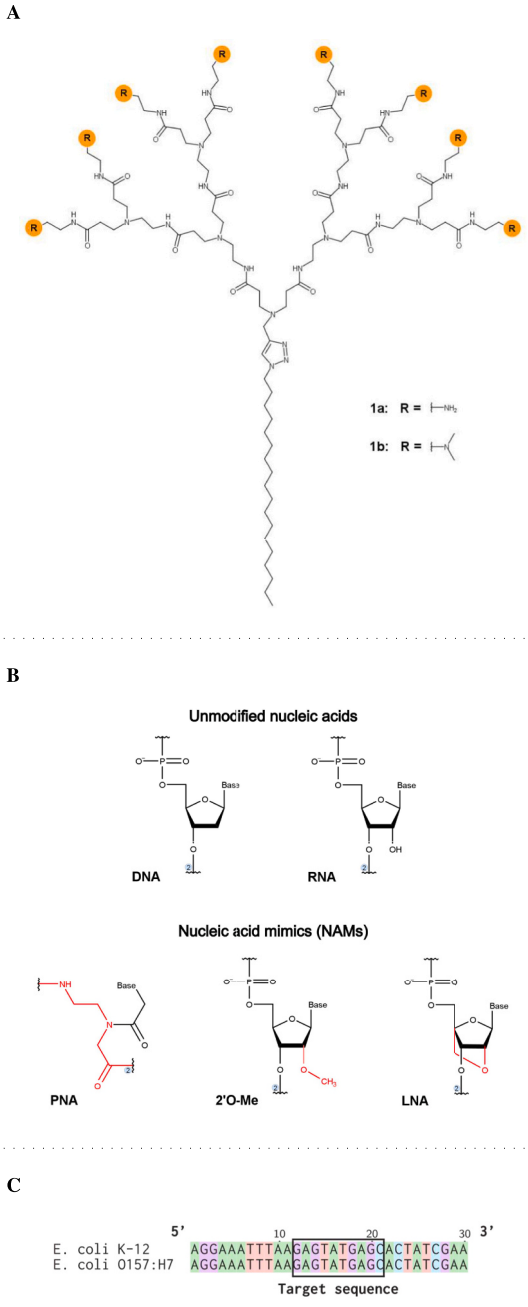

Fig. 1. (A) Chemical structure of the amphiphilic dendrimers used in this study. The ADs 1a and 1b differ only in their functionalisation, with their terminal groups being primary or tertiary amines, respectively. Adapted from Dhumal *et al.* [31] **(B)** Nucleic acid mimic chemistries used in this study (PNA, 2′O-Me and LNA) when compared to the native nucleic acids (DNA and RNA). **(C)** Alignment of an initial portion of the *acpP* gene (and the 15 previous nucleotides) in two fully sequenced *E. coli* strains, with the identification of the selected target.

Regardless of chemistry (Fig. 1B), these NAMs targeted the essential *acpP* gene in *E. coli* (Fig. 1C). First, the ADs and their combination with NAMs were characterised regarding size, zeta potential and loading efficiency. Second, the intrinsic antibacterial activity of the ADs was characterised and their mechanism of action was studied in order to enlighten their function as a delivery vector. Third, AD-assisted NAM internalisation and the resulting antibacterial activity were evaluated *in vitro*. Lastly, the most promising formulations were evaluated regarding their toxicity, using a *Galleria mellonella in vivo* model.

2. Results and discussion

2.1. Characterisation of ADs and AD-NAMs

A comprehensive physicochemical characterisation of the ADs and AD-NAM formulations was conducted. Transmission electron microscopy (TEM), electrophoretic light scattering (ELS), and size exclusion chromatography (SEC) were used to respectively assess their size, zeta potential, and loading efficiency (Table 1).

All formulations presented micellar structures (Fig. 2 and Fig. A.1 in Supplementary Data) with sizes in the nanometer range, consistent with previous reports for the ADs alone [31,32]. While, through visual inspection, some larger micelles were found ($\geq$ 50 nm), all formulations presented the bulk of particles in the 5–30 nm range (Table 1 and Fig. A.2 in Supplementary Data).

Regarding colloidal stability (Table 1), the zeta potential of the ADs alone indicated moderate stability (10 to 30 mV) in solution. Additionally, it revealed an associated net positive charge ($>$ 0 mV), as expected for amine-functionalised compounds. With 1b presenting a lower value than 1a, these results are consistent with what has been previously reported in the literature [31,32]. When combined with the PNA-based NAMs, the formulations maintained a net positive charge ($>$ 0 mV). Notably, for both 1a and 1b, adding PNA-based NAMs led the zeta potential to converge towards 20 to 22 mV, maintaining appropriate colloidal stability. Additionally, the estimated loading efficiencies (Table 1) indicate a high level of interaction between ADs and the PNA-based NAM. This association is maintained over time, with a slight but non-significant drop verified at 24 h (Fig. A.4 A in Supplementary Data). This behaviour is consistent with the aforementioned stability. Alternatively, when combined with the LNA-based NAMs, the formulations presented a net negative charge ($<$ 0 mV), agreeing with the addition of the negatively charged compound. However, both formulations presented a low magnitude of potential (0 to $\pm$ 10 mV), indicating reduced stability. Notably, when assessing the formulations with Cy3-labelled LNA-based NAMs, the accumulation of a gel-like precipitate was observed at the bottom and on the walls of the microtubes (Fig. A.5 in Supplementary Data). This observation further supported the zeta potential results, demonstrating unfavourable colloidal stability. While this behaviour is in line with low zeta potential systems (0 to $\pm$ 10 mV), it severely impacted the loading efficiency estimates, as these are dependent on having both complexed and free NAMs in solution. The LNA-based AD-NAM complexes likely aggregate and eventually precipitate, and are therefore not quantifiable through this method. Even though it was not possible to quantify this complexation, the steep drop of total fluorescence in the LNA-based AD-NAM solutions during the first hours of incubation (Fig. A.4D in Supplementary Data) allied to the presence of virtually only free LNA in solution (Fig. A.4B in Supplementary Data), suggest a substantial level of complexation between the ADs and the LNA-based sequence.

Table 1
Characterisation of the ADs and AD-NAMs used in this study.

ID	Particle size[a] [nm]	Zeta potential[b] [mV]	Loading efficiency[c] [%]
1a	14 ± 7.4	29.1 ± 1.3	n/a[d]
1a-LNA	14 ± 8.9	− 9.2 ± 0.3	n/q[e]
1a-PNA	11 ± 5.8	22.2 ± 1.1	59.8 ± 10.8
1b	13 ± 8.1	12.0 ± 0.8	n/a[d]
1b-LNA	12 ± 7.3	− 5.7 ± 1.3	n/q[e]
1b-PNA	12 ± 6.3	20.5 ± 1.0	71.0 ± 0.9

[a] Particle size refers to the obtained Feret diameter measurements. The mean and standard deviation are presented for particles detected through semi-automated segmentation using twelve images (minimum) per formulation.
[b] The mean and standard deviation of three repeated measurements (minimum) are presented.
[c] The mean and standard deviation of three independent experiments are presented.
[d] n/a: Not applicable.
[e] n/q: Not quantified. As AD-NAM precipitation was detected and its attachment to the microtube surface was verified, estimated values for LNA-based formulations based on SEC are heavily skewed, not allowing a representative quantification.

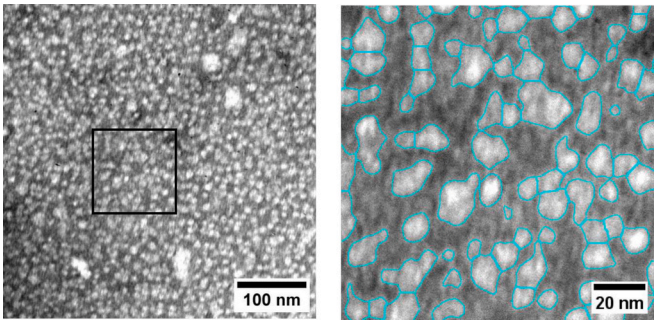

Fig. 2. Transmission electron micrographs of the complexes formed by the AD 1a with the LNA-based NAM (LNA), as an example of the obtained structures. The micrograph on the right corresponds to a zoomed-in view of the area highlighted in the image to its left. Outlines in blue indicate the boundaries of the particles, as detected through semi-automated segmentation. Micrographs for all ADs and AD-NAMs are available in Fig. A.1 in Supplementary Data. (For interpretation of the references to colour in this figure legend, the reader is referred to the web version of this article.)

2.2. Determination of the sub-lethal dose of the ADs

An intrinsic antibacterial effect against *E. coli* was expected for both ADs [32,44,45]. However, to take full advantage of the AD-mediated NAM delivery strategy, it was necessary to select a sub-lethal concentration of the ADs at which they can primarily assist as delivery vectors rather than act as antibacterials.

To do so, traditional microdilution-based methods were used to determine the minimal inhibitory concentration (MIC) leading to a reduction of at least 80 % in growth (MIC_{80}). Both ADs resulted in MIC_{80} values of 18.8 μM (Fig. 3A and Fig. A.6 A in Supplementary Data). The minimum bactericidal concentration (MBC) was determined as 2 × MIC_{80}, i.e., 37.5 μM for both ADs (Fig. 3A). Previous studies reported lower MIC_{50} values, namely 3.1 and 2.8 μM against *E. coli* for 1a and 1b, respectively [32,44]. These differences are possibly due to variations in the protocol such as the use of different target strains, media, reporting levels, or initial bacterial concentrations. For confirmation, an evaluation on the impact of media (LB vs MHB) and reporting levels (MIC_{80} vs MIC_{50}) in MIC values was conducted, and the obtained data corroborated this hypothesis (Fig. A.7 in Supplementary Data).

To examine the range of activity of the ADs, a similar assessment was performed for *B. subtilis* and *S. epidermidis* (Fig. A.8 in Supplementary Data). When compared to the results for *E. coli*, the MIC_{80} was higher for *S. epidermidis* (37.5 μM for 1a and 75.0 μM for 1b) and equal or lower for *B. subtilis* (18.8 μM for 1a and 9.4 μM for 1b). These results demonstrate the inherent variability in AD activity across different bacterial species, without an apparent correlation to Gram type. This activity is likely species-dependent as a result of envelope variability, as ADs have been reported to target phosphatidylglycerol and cardiolipin [44].

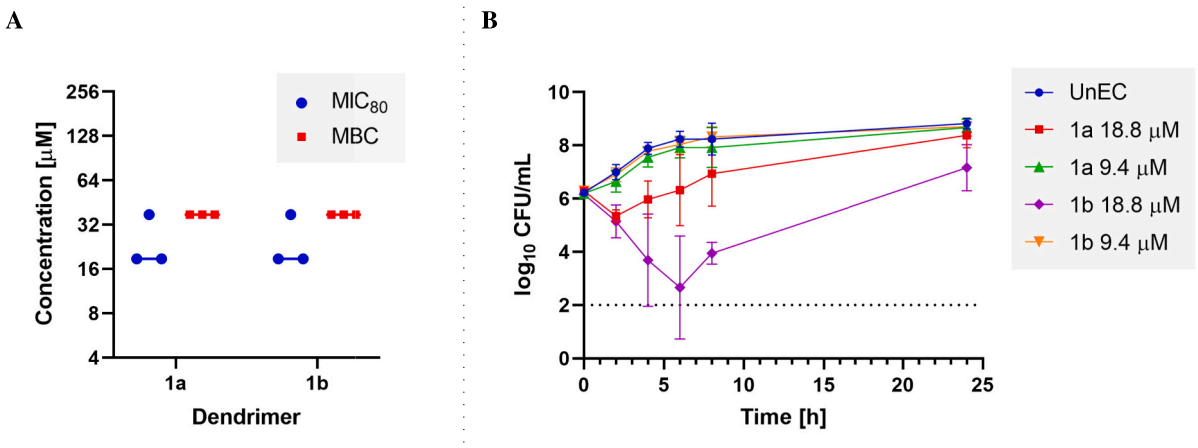

Fig. 3. Evaluation of the inhibitory effect of the amphiphilic dendrimers. **(A)** Minimum inhibitory and bactericidal concentrations (MIC_{80} and MBC, respectively) in *E. coli* ATCC 25922 for both ADs in study. The individual values and the median of three independent experiments are presented. **(B)** Time-kill kinetics of 1a and 1b at MIC_{80} and sub-MIC_{80} concentrations for 24 h, when compared with normal *E. coli* growth (UnEC). The mean and standard deviation of three independent experiments are presented. The dotted line indicates the method's detection limit (2 $\log_{10}$ CFU/mL). The determined MICs (18.8 μM for both 1a and 1b) ensure the impact of the ADs in the *E. coli* population and were therefore selected for subsequent experiments.

Additionally, the envelope of bacteria from the *Staphylococcus* genus is generally harder to translocate, as verified in applications such as traditional FISH and liposome-assisted delivery [24,46,47].

To further assess the effect of the ADs in an *E. coli* population over time (Fig. 3B), bacterial colony forming units were quantified over 24 h of incubation at MIC_{80} and sub-MIC_{80} concentrations (18.8 μM and 9.4 μM, respectively). Observable reductions were obtained only at MIC_{80} concentrations, with 1b showing a more pronounced activity (after 6 h of incubation, 1.9 ± 1.3 $\log_{10}$ reduction for 1a vs 5.6 ± 1.9 for 1b). In fact, when considering the 24 h of incubation, a significant bacterial reduction was only detected for 1b at MIC (Fig. A.6B in Supplementary Data). Additionally, the time-kill curves revealed an initial bacterial load reduction, lasting up to 6 h, followed by a recovery in the growth of *E. coli*. These results indicate a bactericidal behaviour with a dwell time in the hour range. The recovery may be a direct consequence of the mechanism of action underlying the ADs' antibacterial activity, as recent findings indicate they interact with and disrupt the bacterial membrane [32,44,48]. If this interaction is maintained with dead cells and/or membrane components, their repeated action is limited and will not reach the remaining bacterial population. Alternatively, recovery could stem from bacterial membrane repair mechanisms [49–52] or the survival of a subpopulation less affected by the ADs, a phenomenon commonly observed in bacterial stress responses [53–57].

The determined MICs (18.8 μM for both 1a and 1b) ensure the impact of the ADs in the bacterial population (detectable through turbidity and colony counts) and remain at a sub-lethal level, providing a considerable margin to detect changes in antibacterial activity when employing the ADs as delivery vectors. These concentrations were therefore selected for subsequent experiments.

2.3. AD-promoted membrane permeabilisation

The ADs' permeabilisation of *E. coli*'s bacterial envelope was assessed using flow cytometry (FC) and TEM, to improve our understanding of their mechanism of action.

First, propidium iodide (PI) was used to stain *E. coli* cells in order to quantify the level of membrane permeabilisation using FC. PI is a fluorescent molecule which can easily enter permeabilised membranes and bind to DNA emitting red fluorescence, allowing the distinction of these two populations (intact vs permeabilised) [58,59]. In the PI staining experiments, untreated *E. coli* (UnEC) was used as the negative control, whereas two treatments were used as positive controls: i) polymyxin (Poly), an antibiotic that acts on Gram-negative membranes [60,61]; and ii) ethanol (EtOH), a common permeabiliser in microbiology protocols [62]. As expected, the negative control resulted in minor staining (11 ± 2.5 % for UnEC) while the positive controls led to near total staining of the bacterial population (92 ± 6.9 % for polymyxin and 96 ± 5.2 % for ethanol) (Fig. 4A), with the corresponding histograms, showing high-intensity PI-stained populations (Fig. 4B). Incubating the ADs with *E. coli* for 15 min at their MIC_{80} resulted in increased bacterial permeabilisation when compared with untreated *E. coli* (Fig. 4). Interestingly, 1b led to a higher percentage of PI-stained cells (82 ± 3.3 %) when compared to 1a (45 ± 0.87 %) (Fig. 4A). This difference in permeabilisation observed for 1a and 1b highlights the role of surface functionalisation. The tertiary amine terminals in 1b present not only a strong tendency for protonation but also a higher lipophilicity than the primary amines located at the surface of 1a, potentially increasing the interaction with the overall negatively charged bacterial envelope and leading to enhanced permeabilisation. The balancing of these results with the ADs' zeta potentials (Table 1) further highlights the importance of lipophilicity, as the overall charge alone was not the decisive factor for this behaviour.

To further investigate the interaction of the ADs with the bacterial envelope, TEM was used to visually inspect *E. coli* upon incubation with 1a and 1b. The treatment with polymyxin was used as the positive control. In Figs. 5B-C, the micrographs show prominent AD-induced changes to the bacterial structure and/or its surroundings. These results contrast those of untreated bacteria (Fig. 5A) which, as expected, have a consistently dense cytosol and present a well-defined and intact cell envelope (outer membrane, cell wall and plasma membrane). While no obvious changes seemed to be caused by 1a to the bacterial envelope (Fig. 5B), an accumulation of high electronic density material is observed in the field of view, mainly near bacteria. These agglomerates might correspond to i) the debris of dead cells or ii) the supramolecular structures formed by the ADs in solution, especially at high local concentrations promoted through electrostatic interactions with bacteria. This second hypothesis is supported by the visualisation of the ADs alone at a high concentration (2 mM) which revealed similar agglomerates (Fig. A.9 in Supplementary Data). In Fig. 5C, portraying 1b-treated *E. coli*, changes in the bacterial envelope are evident. While some bacteria still appear intact, a considerable portion of the observed cells revealed the lack of an outer membrane accompanied by a fuzzy appearance at the expected envelope location. This closely matches the disruption of the outer membrane verified for polymyxin-treated *E. coli* (Fig. 5D). The increased disruption caused by 1b (over 1a) is coherent with their overall antibacterial effect (Fig. 3B) as well as their effect on

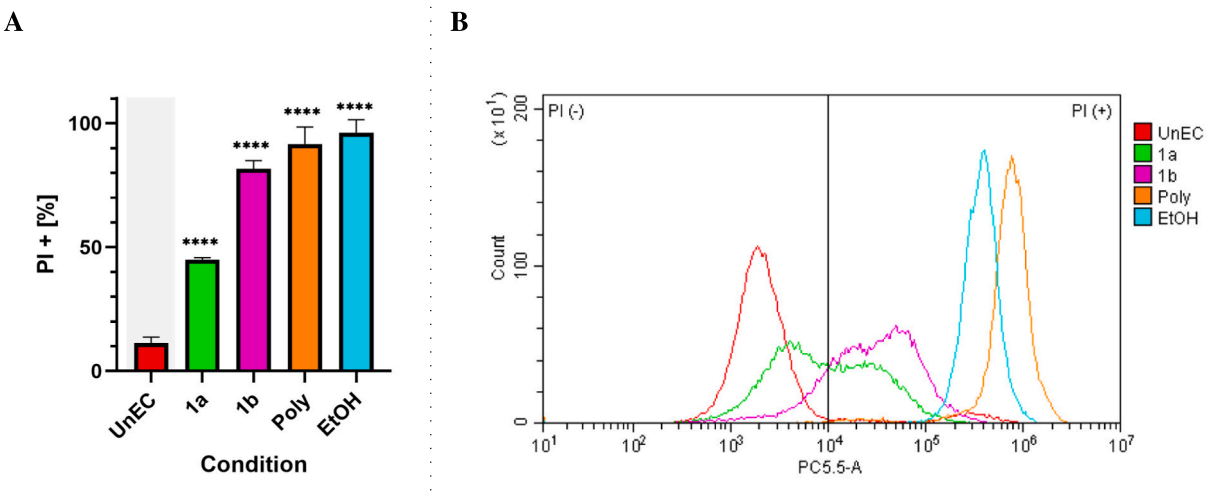

Fig. 4. Flow cytometry for the evaluation of membrane permeabilisation. **(A)** The percentage of PI-stained *E. coli* ATCC 25922 cells after incubation with the ADs (1a or 1b) for 15 min is presented; *E. coli* cells incubated with polymyxin (Poly) or previously permeabilised with ethanol (EtOH) were used as positive controls; untreated *E. coli* (UnEC) was used as a negative control. The mean and standard deviation of three independent experiments are presented. Statistical differences, in comparison to untreated *E. coli* (background in grey) and determined via one-way ANOVA, are indicated when appropriate in * ($p \leq 0.0001$, ****). **(B)** A representative histogram overlay is presented, illustrating the fluorescence intensity profiles of the selected conditions. The vertical gate for PI internalisation was defined at 10^4 arbitrary fluorescence units (AFU), as demonstrated by the vertical line. Both ADs led to significant bacterial permeabilisation, with 1b leading to a higher percentage of PI-stained cells than 1a.

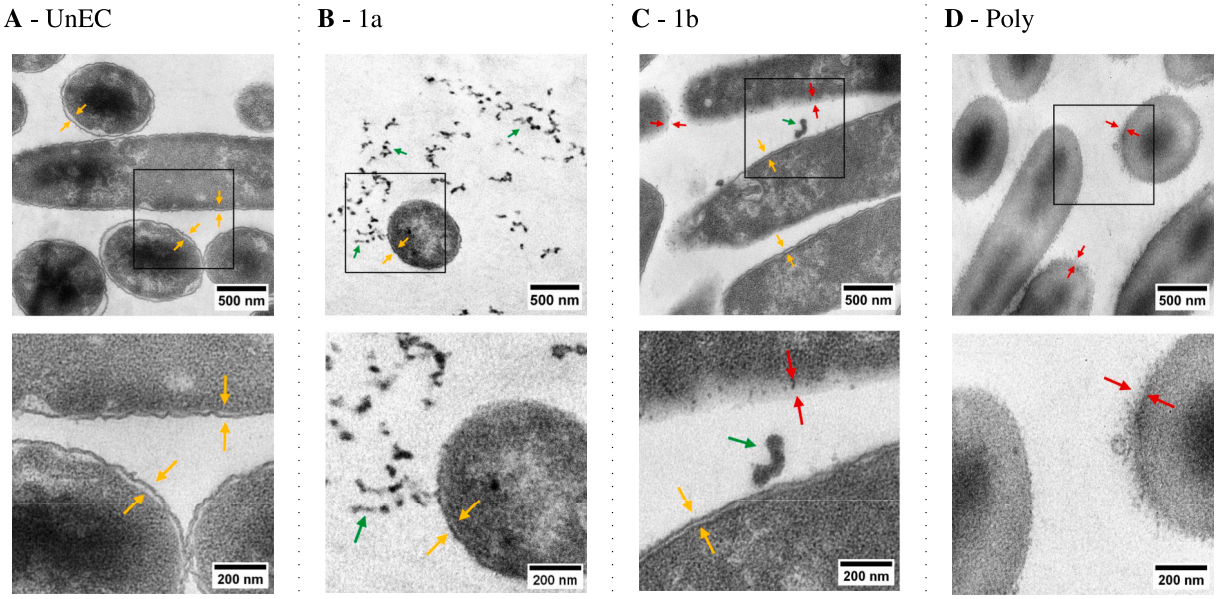

Fig. 5. Transmission electron micrographs of *E. coli* ATCC 25922 cells: **(A)** untreated bacteria (UnEC); bacteria treated with **(B)** 1a or **(C)** 1b (at MIC_{80}) for 2 h; **(D)** polymyxin (Poly) was used as a positive control, leading to complete disruption of the bacterial outer membrane. Each micrograph in the bottom row corresponds to a zoomed-in view of the area highlighted in the image directly above it. Coloured arrows indicate the intact bacterial envelope (in yellow), no distinct outer membrane accompanied by fuzziness at the envelope (in red), and high electronic density material accumulated in the focal plane (in green). AD-induced changes to the bacterial structure and/or its surroundings corroborate their role as envelope permeabilisers. (For interpretation of the references to colour in this figure legend, the reader is referred to the web version of this article.)

membrane integrity as determined via FC (Fig. 4). Interestingly, the presence of nearby agglomerates was less common for bacteria exposed to 1b than for 1a-treated bacteria. It has been proposed that AD micelles disassemble while penetrating the bacterial envelope [32,44]. The increased activity, membrane permeabilisation and reduction of visible agglomerates for samples of *E. coli* exposed to 1b support this proposed mechanism. These results also reveal the nuanced nature of comparing compounds through MIC. Despite presenting similar MIC values, there is a clear discrepancy between the ADs' action as envelope permeabilisers, already glimpsed through their activity over time (Fig. 3B). This contrast between MIC and permeabilisation could be mainly attributed to i) the sensitivity and threshold effect of the MIC determination method, and ii) time dependency and assay nature, given that MICs are determined after 24 h of exposure, while permeabilisation was evaluated after only 15 min or 2 h of incubation, for FC and TEM respectively.

Collectively, both FC and TEM imaging results indicate the partial permeabilisation of the bacterial envelope caused by the ADs.

2.4. AD-assisted NAM internalisation

The next step was to assess whether the AD-promoted permeabilisation would potentiate the internalisation of NAMs when applied as a combined formulation (AD-NAMs). To achieve this, the LNA- and PNA-based NAMs targeting the *acpP* gene were labelled with the fluorophore Cy3. FC and epifluorescence microscopy were used to evaluate the internalisation in *E. coli* of the Cy3-labelled NAMs when complexed with each of the ADs (Figs. 6 and 7, respectively). The results were compared with free NAMs as well as PNA conjugated to the cell-penetrating peptide $(KFF)_3K$ (named as POC hereafter), a conjugate known to successfully transport NAMs and inhibit bacterial growth [14].

The FC-based quantification of Cy3-stained cells (Fig. 6A) revealed both ADs led to significant NAM internalisation, particularly for LNA-based NAMs. As expected, the NAMs alone stained a residual fraction of the *E. coli* population (up to 3.4 ± 3.5 % cells for PNA), while the peptide-NAM conjugate resulted in a near complete staining (95 ± 3.3 % cells for POC). In general, 1a was more successful (90 ± 15 % cells for 1a-LNA) than 1b (50 ± 22 % cells for 1b-LNA) as an assistant of NAM internalisation, while LNA showed superior internalisation when compared to PNA (54 ± 25 % cells for 1a-PNA and 20 ± 3.5 % cells for 1b-PNA). Notably, both NAM chemistry and ADs were considered significant factors, with the ADs accounting for over 40 % of variation in NAM internalisation (Fig. A.10 and Table A.1 in Supplementary Data).

The FC spectra were further analysed by calculating the median of orange fluorescence obtained for each sample (Fig. 6B). As expected, the samples which led to statistically improved bacterial staining in Fig. 6A revealed a median above 4 log arbitrary fluorescence units (AFU). This value was selected as the threshold for Cy3 internalisation as it corresponds to the maximum detected fluorescence for UnEC. Interestingly, it also allowed the distinction between two groups above this threshold: lower intensity, verified for 1b-LNA and 1a-PNA (up to 5 $\log_{10}$ AFU), and higher intensity, verified for 1a-LNA and POC (above 5 $\log_{10}$ AFU). This denotes a variation in fluorescent intensity of approximately tenfold, which is presumed to be noticeable when imaging these samples through a fluorescent microscope.

Fluorescence microscopy (Fig. 7) showed the untreated bacteria (UnEC) stained blue corresponding to the DAPI counterstain, demonstrating the presence of *E. coli*. Similarly, the samples for LNA, PNA and 1b-PNA showed only blue-stained cells, indicating the reduced internalisation of the labelled NAMs in *E. coli*. As predicted from Fig. 6B, 1a-PNA and 1b-LNA presented a low level of Cy3 staining (orange), which results in a purple hue when combined with the DAPI counterstain. The samples with the highest Cy3 intensity (1a-LNA and POC) presented strongly pink-stained cells, highlighting the increased NAM internalisation. These images corroborate the results obtained via FC (Fig. 6).

Overall, LNA-based formulations presented higher internalisation when compared to their PNA counterparts. Electrostatic and other forces predictably play a role in these events, both within the AD-NAM complexes and when reaching the bacterial envelope. So far, most approaches to enhance NAM bacterial uptake have been based on the conjugation of PNA with carriers (e.g., cell-penetrating peptides or vitamin B12) [63]. As such, the role of charge in AD-NAM complexation and activity remains unclear; however, some inferences can be made. Negatively charged sequences, such as the LNA/2'OMe chimaera, likely interact more strongly, through electrostatic interactions, with the cationic ADs than neutrally charged sequences. The substantial reduction of labelled NAMs in solution, verified for LNA-based formulations, is consistent with a high level of complexation (Figs. A.4D and A.5 in Supplementary Data). This inference is reinforced by the parallel with anionic siRNA, which has been successfully complexed with these ADs for delivery in mammalian cells [28,30,31,33,35]. Nonetheless, the neutral PNA-based sequence successfully associates with the ADs, with moderate to high loading efficiencies (Table 1 and Fig. A.4 A in Supplementary Data). This interaction is likely driven by hydrogen bonds, hydrophobic and van der Waals forces, of a weaker nature [64–66]. Besides AD-NAM interaction, NAM binding affinity with the target RNA sequence is also relevant. While LNA-based sequences have been suggested to provide higher affinities than those with PNA, this conjecture has not yet been fully established [67,68]. Additionally, the precipitation witnessed for LNA-based complexes adds a layer of complexity to the interpretation of these results. The process of complex formation, aggregation and precipitation is predictably ongoing during the first few hours of contact with bacteria, as detected in solution free of bacteria (Fig. A.4D in Supplementary Data). With this phenomenon, a lower

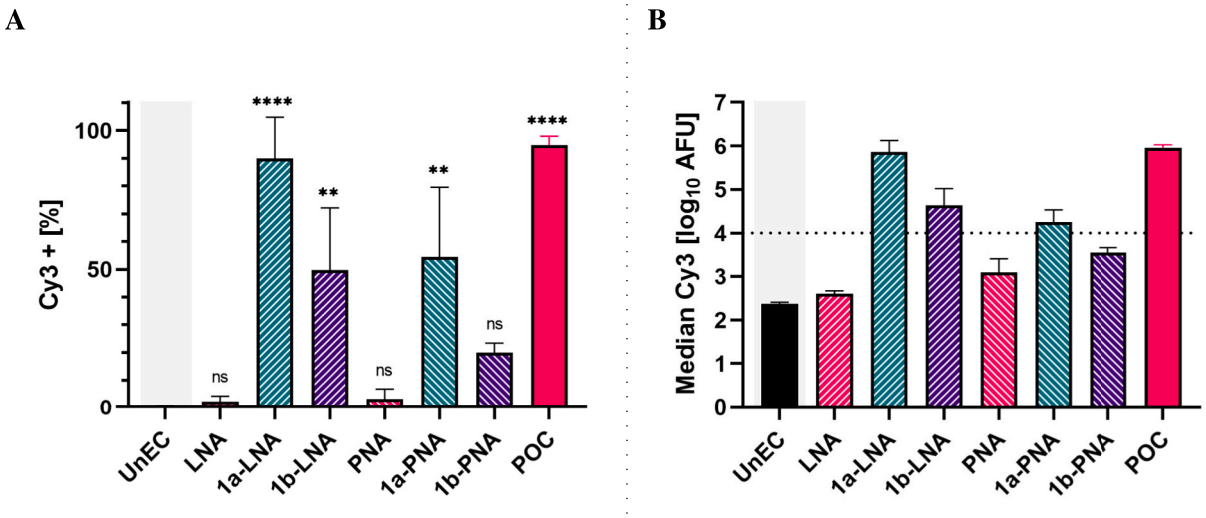

Fig. 6. Flow cytometry for the evaluation of NAM internalisation. **(A)** The percentage of Cy3-stained *E. coli* ATCC 25922 cells after incubation with the AD-NAM complexes (for 15 min) is presented and grouped according to the antisense compound: the LNA-based NAM (LNA) or the PNA-based NAM (PNA). *E. coli* cells exposed to the peptide-oligonucleotide conjugate (POC) were used as a positive control. The mean and standard deviation of three independent experiments are presented. Statistical differences, in comparison to untreated *E. coli* (background in grey) and determined via one-way ANOVA, are indicated when appropriate in * ($p > 0.05$, ns; $p \leq 0.01$, **; $p \leq 0.0001$, ****). **(B)** The median of orange fluorescence intensity is presented and grouped according to the antisense compound. The dotted line (defined at 4 $\log_{10}$ AFU) indicates the selected threshold gate for Cy3 internalisation, corresponding to the maximum detected fluorescence for UnEC. Both ADs enhanced Cy3-labelled NAM internalisation in *E. coli* (particularly for LNA-based NAMs).

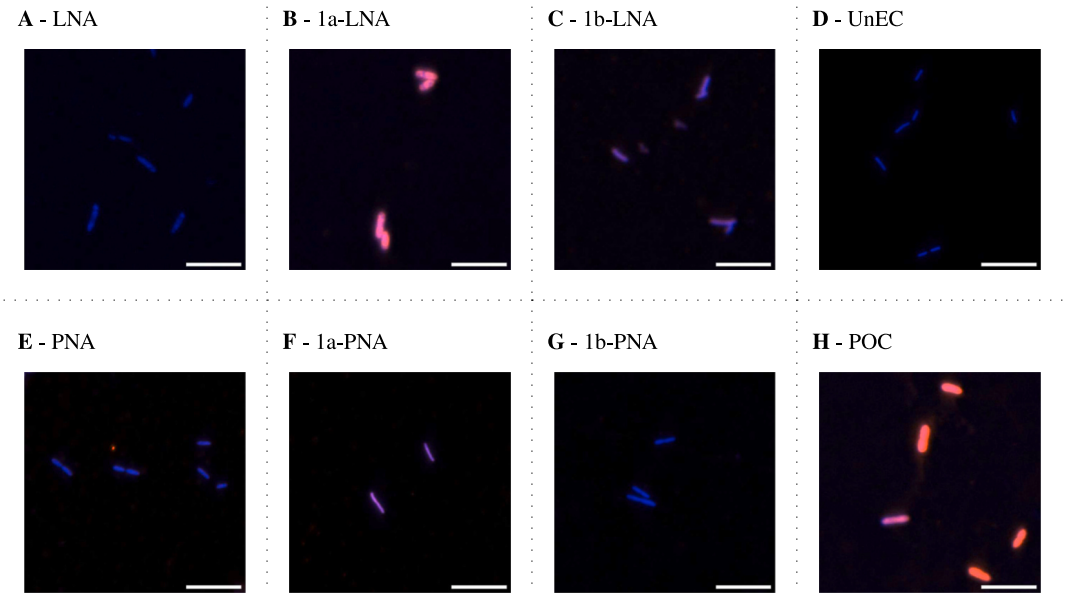

Fig. 7. Fluorescence micrographs of *E. coli* ATCC 25922 cells incubated with the various AD-NAM complexes. *E. coli* was incubated with one of the ADs (1a or 1b), previously complexed with the Cy3-labelled **(A-C)** LNA-based NAM (LNA) or the **(*E*-G)** PNA-based NAM (PNA). **(D)** Untreated *E. coli* (UnEC) was used as a negative control. To guarantee NAM internalisation and assess maximum fluorescence, *E. coli* was visualised after exposure to **(H)** the peptide-oligonucleotide conjugate (POC), as a positive control. All samples were subject to a DAPI counterstain in order to visualise bacteria. The scale bar represents 10 μm. These images corroborate the results obtained via FC, showing both ADs enhance NAM internalisation in *E. coli*.

number of complexes are expected to be available to bind to the bacteria and subsequently be internalised, potentially implying a decrease in the detected fluorescence. However, given this analysis was performed after 15 min of bacterial exposure to the AD-NAMs, the authors hypothesise a substantial amount of both AD, NAMs, and the resulting complexes are still in solution, limiting this impact. On the other hand, the aggregation may even contribute to an artificial increase of the detected fluorescence. Ultimately, the higher fluorescence signal detected for LNA-based formulations is a direct consequence of AD-NAM complexation and internalisation allied to the dynamic aggregation of the complexes (i.e., before precipitation). Regarding the ADs, although 1b previously demonstrated improved envelope permeabilisation over 1a (Figs. 4 and 5), it led to a less pronounced internalisation of the NAMs than 1a. It is likely that, given 1b's higher lipophilicity and strong tendency for protonation, the forces established with the NAMs and the negatively charged outer membrane of the envelope are more robust to overcome than those of 1a. While zeta potential measurements of the complexes do not indicate a strong dependency on the AD, loading efficiency values lean towards a slightly higher tendency for complexation of 1b than that of 1a. These forces may limit the effective traversal of the labelled NAMs into the bacterial cytosol, potentially clarifying the reduced cell staining associated with 1b. Lastly, it is worth noting the considerable success of 1a-LNA, which demonstrated a level of internalisation comparable to that of already established vectors. Besides the POC used in this study, 1a-LNA presented values similar to or higher than those obtained for NAM-loaded liposomes (varying from 30 to 100 % delivery efficiency, after 24 h), previously tested by our group [23,47]. Although this study's primary goal is the use of AD-NAMs as a therapeutic alternative, these internalisation results highlight the potential of this strategy for diagnostic applications. Amphiphilic dendrimers could be used for the delivery of labelled NAMs, namely those targeting species-specific genes, and allow the identification of specific pathogens in complex bacterial samples.

2.5. AD-NAMs effect on bacterial viability

Having shown that both ADs can permeabilise the bacterial envelope and deliver the antisense NAMs, we aimed to investigate if the delivered antisense NAMs could effectively kill bacteria. In order to assess the antibacterial effect, *E. coli* colonies were quantified over a period of 24 h of incubation with the selected formulations. In combination with either AD, the previously mentioned LNA- and PNA-based NAMs were studied. To exclude non-specific effects, a PNA-based scrambled sequence (Scr) was used as a negative control.

For the formulations with 1a (Figs. 8A-B), the combinations with LNA and Scr both led to very similar results to those verified for 1a alone (e.g., $\log_{10}$ reduction after 8 h of 2.8 ± 0.32 for 1a-LNA, 2.9 ± 1.2 for 1a-Scr and 2.5 ± 1.5 for 1a). Despite maintenance of the bacterial load throughout the first few hours, these formulations (1a, 1a-LNA and 1a-Scr) led to a recovery at the end of the incubation period that was similar to values obtained for normal bacterial growth (UnEC). Only the combination with PNA led to a noticeable reduction (e.g., 6.3 ± 1.8 $\log_{10}$ reduction after 8 h for 1a-PNA), highly pronounced after only 6 h, which was maintained up to 24 h.

The formulations with 1b (Figs. 8C-D) revealed a more pronounced effect than those with 1a, as expected given its increased intrinsic activity and coherently with the added envelope permeabilisation (shown in Sections 2.2 and 2.3). The combinations of 1b with LNA and Scr led to a seemingly improved effect over the AD alone (e.g., $\log_{10}$ reduction after 8 h of 5.9 ± 1.6 for 1b-LNA and 6.0 ± 2.0 for 1b-Scr vs 4.2 ± 2.0 for 1b). However, when comparing formulations after 8 h of incubation, only the combination with PNA effectively resulted in a statistically significant antibacterial improvement (e.g., 7.5 ± 1.4 $\log_{10}$ reduction after 8 h for 1b-PNA). Nonetheless, when analysing the overall effectiveness (Fig. A.11 in Supplementary Data), using the area under the time-kill curves, 1b-LNA also showed statistical differences to 1b alone. For comparison, POC leads to an intense decrease during the first 4 h, after which there is also a bacterial recovery, even more pronounced than that verified for the active AD-NAM formulations (Fig. A.11C in Supplementary Data).

Altogether, these results reveal a significant enhancement in antibacterial activity when the anti-*acpP* PNA sequence is used, assisted by either of the ADs. With a very significant bacterial load reduction (up to 8 $\log_{10}$ CFU/mL), this activity is comparable to those of peptide-PNAs (7 to 8 $\log_{10}$ reduction at 24 h of incubation against UPEC) as reported by Popella *et al.* [13] Additionally, the PNA sequence consistently

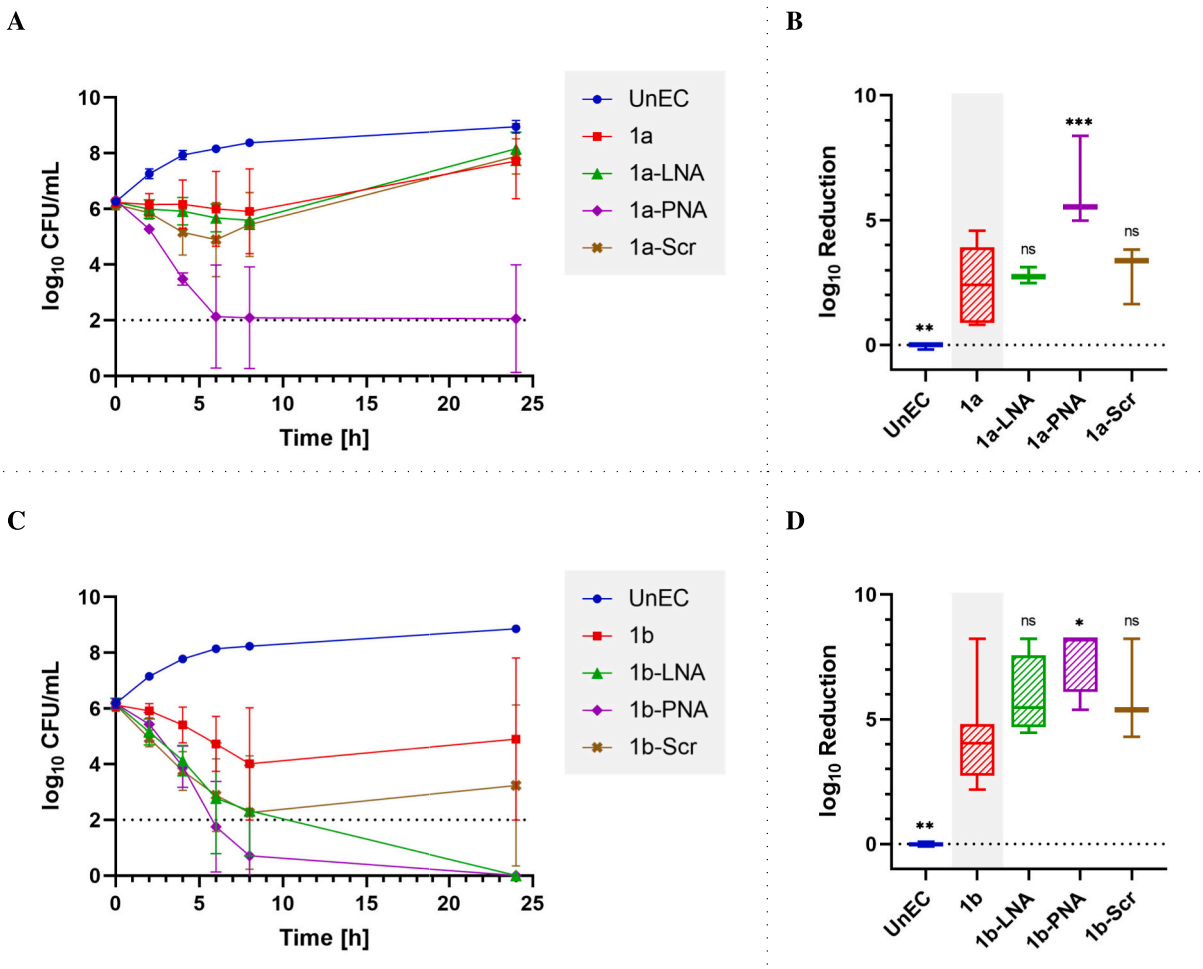

Fig. 8. Evaluation of the inhibitory effect of the AD-NAM complexes against *E. coli* ATCC 25922. **(A and C)** Time-kill kinetics, up to 24 h, of the AD-NAM complexes, based on 1a and 1b, respectively, when combined with the LNA-based NAM (LNA), the PNA-based NAM (PNA), or the PNA-based scramble sequence (Scr), and in comparison to normal *E. coli* growth (UnEC). ADs were evaluated at MIC_{80} (18.8 μM) and combined with NAMs at 15.0 μM. The mean and standard deviation of at least three independent experiments are presented. The dotted line indicates the method's detection limit (2 $\log_{10}$ CFU/mL). **(B and D)** Bacterial reduction (in a $\log_{10}$ scale) after 8 h of incubation for each condition, as represented through a box and whiskers (min to max), with a line at the median. Statistical differences, in comparison to AD-treated *E. coli* (background in grey) and determined via one-way ANOVA, are indicated when appropriate in * ($p > 0.05$, ns; $p \leq 0.05$, *; $p \leq 0.01$, **; $p \leq 0.001$, ***). Antibacterial activity was significantly enhanced when the anti-*acpP* PNA sequence was used, assisted by either of the ADs.

outperformed the scrambled sequence of the same chemistry, confirming the antisense mechanism in play. These results also indicate that, despite lower apparent internalisation, the PNA chemistry is more effective in its anti-*acpP* effect than its LNA-based counterpart. The complex precipitation verified for the Cy3-labelled LNA-based AD-NAM formulations likely has a role in their lack of prolonged activity. While this behaviour was not apparent with non-labelled formulations, the decrease of AD-NAMs in solution, thus reducing effective treatment against *E. coli*, is consistent with the observed recovery in growth and similarity of the time-kill curves to those of the AD alone. Additionaly, while LNA more readily reaches the cytosol through this strategy (as indicated by the FC and fluorescence microscopy results, Figs. 6 and 7), it is possible that its likely stronger complexation to the ADs ultimately hinders its release from the complexes and, consequently, its interaction with the target sequence. Contrarily for PNA, the reduced electrostatic interaction with the ADs, given its neutral charge, may result in a higher availability near its *acpP* target. This tendency has also been reported for peptide-oligo conjugates, for which only PNA revealed antibacterial activity, despite both PNA and LNA-based oligos being strong translation inhibitors (in a cell-free system) [69]. For future studies, the LNA/2-O'Me-based sequence may be further modified, for example, by including amino-modified LNAs, impacting its global charge and potentially its colloidal stability [70,71].

This assessment revealed promising antibacterial formulations, namely those containing PNA-based NAMs, while highlighting the potential of the antisense strategy.

2.6. AD-NAMs against clinical isolates and in vivo

In order to complement this strategy, this proof of concept had to be translated to more clinically relevant conditions. As such, the next steps consisted in i) the *in vitro* evaluation of all AD-NAM formulations against an *E. coli* clinical isolate and ii) the determination of their biocompatibility in a greater wax moth (*Galleria mellonella*) model.

Predictably, all formulations showed less activity against the multi-resistant *E. coli* isolate (H26) than that verified for ATCC 25922 (Fig. 9). The AD 1a by itself showed no antibacterial activity at the used concentrations; however, its permeabilising effect seems to have assisted in the partial internalisation of PNA, contributing to its observable antibacterial activity, noticeable only during the first 8 h (Fig. 9A). Indeed, only the combination with PNA resulted in a minimal but statistically significant bacterial reduction after 8 h (0.68 ± 0.94 $\log_{10}$ reduction after 8 h for 1a-PNA) (Fig. 9B). Even so, none of the 1a-assisted formulations led to significant activity when considering the entire

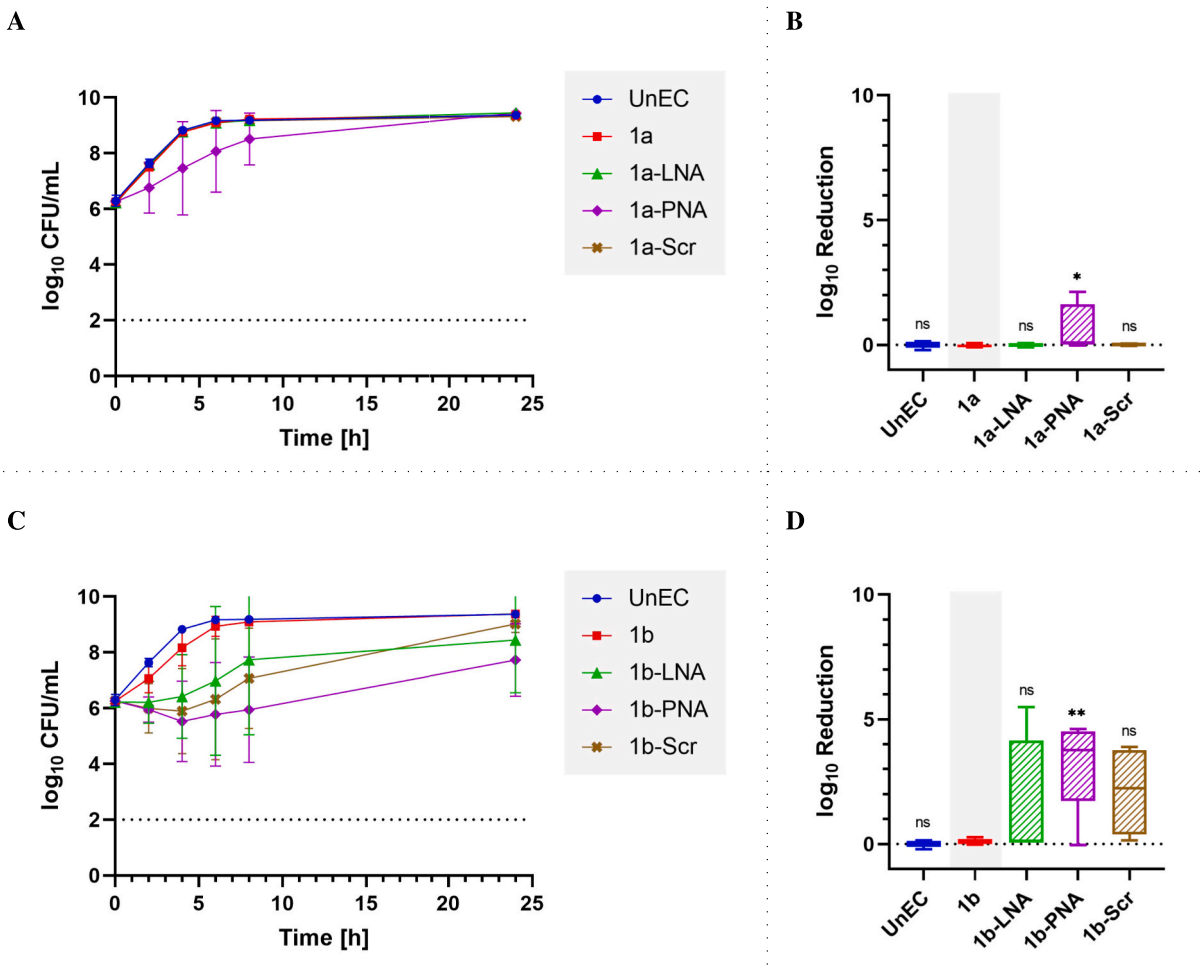

Fig. 9. Evaluation of the inhibitory effect of the AD-NAM complexes against *E. coli* H26. **(A and C)** Time-kill kinetics, up to 24 h, of the AD-NAM complexes, based on 1a and 1b, respectively, when combined with the LNA-based NAM (LNA), the PNA-based NAM (PNA), or the PNA-based scramble sequence (Scr), and in comparison to normal *E. coli* growth (UnEC). ADs were evaluated at MIC_{80} (18.8 μM) and combined with NAMs at 15.0 μM. The mean and standard deviation of at least three independent experiments are presented. The dotted line indicates the method's detection limit (2 $\log_{10}$ CFU/mL). **(B and D)** Bacterial reduction (in a $\log_{10}$ scale) after 8 h of incubation for each condition, as represented through a box and whiskers (min to max), with a line at the median. Statistical differences, in comparison to AD-treated *E. coli* (background in grey) and determined via one-way ANOVA, are indicated when appropriate in * ($p > 0.05$, ns; $p \leq 0.05$, *; $p \leq 0.01$, **). All formulations showed less activity against the multi-resistant *E. coli* isolate. Nonetheless, the combination of 1b with PNA remained the most promising, still demonstrating significant antibacterial activity.

incubation period (Fig. A.12 in Supplementary Data). Maintaining the previous pattern, formulations with 1b showed overall higher activity (Figs. 9C-D). While 1b's intrinsic antibacterial effect was also barely detectable under these conditions, the combinations with the selected NAMs led to some improvements (e.g., $\log_{10}$ reduction after 8 h of 1.5 ± 2.7 for 1b-LNA and 2.1 ± 1.8 for 1b-Scr vs 0.096 ± 0.11 for 1b). Nonetheless, the combination with PNA remained the most promising, as the only leading to significant effects (e.g., 3.2 ± 1.9 $\log_{10}$ reduction after 8 h for 1a-PNA), for activity after 8 h (Fig. 9D) as well as when regarding its effectiveness over time (Fig. A.12 in Supplementary Data). Similarly, POC activity is also diminished against this isolate, with a slight antibacterial effect during the first 4 h, after which there is a recovery of growth, more pronounced than that verified for the active AD-NAM formulations (Fig. A.12C in Supplementary Data).

As opposed to the originally tested *E. coli* strain, the isolate H26 presents resistance to several antibiotics (Table A.2 in Supplementary Data). The resistance to *β*-lactams and tetracyclines suggests some level of porin downregulation or mutation, potentially reducing the uptake of hydrophilic substances (e.g., the NAMs). Additionally, resistance to fluoroquinolones, aminoglycosides, tetracyclines and macrolides is associated with the upregulation of efflux pumps, which may contribute to the displacement of both ADs and NAMs. Lastly, while not directly associated with any of the detected resistances, it is conceivable this isolate also presents envelope differences, which may limit the interaction with ADs and AD-NAMs. The present resistance mechanisms collectively contribute to the reduced antibacterial activity observed in *E. coli* H26.

Nevertheless, these results emphasise a distinct benefit of this strategy. Despite 1b showing no antibacterial activity against H26, the added effect of the PNA sequence in the 1b-PNA formulation leads to an approximately 3 $\log_{10}$ reduction in bacterial load. This decrease results from the permeabilisation caused by the AD, allied to the bacteria-specific antisense action of the PNA. In a clinical context, this pathogen-targeted approach likely allows the preservation of commensal microbiota which is essential for supporting the immune system and reducing the risk of dysbiosis. Additionally, this selective killing reduces the pressure on non-targeted bacteria, likely diminishing the tendency for resistance development. The relatively easy design and tuneability of NAM sequences allow for a universal strategy that can be tailored to other pathogens, maintaining specificity. Towards validation, future studies can include an evaluation of this therapeutic strategy against mixed biofilms, targeting *E. coli* while including other relevant

species.

Given these results, only the formulations with 1b were evaluated regarding their toxicity *in vivo*. For this purpose, the survival and health of *G. mellonella* larvae were monitored after injection with the selected formulations. When injected with the compounds (Fig. 10), no significant toxicity was found regarding either survival ($p = 0.37$) or overall health of the larvae ($p = 0.54$). Some conditions, including the saline control, led to the death of one or two individuals over the 72 h (Fig. 10A); however, this variation is to be expected within the larval life cycle. Additionally, the health index of all groups remained above 6, indicating an overall healthy state of the larvae (Fig. 10B). Our observations regarding biocompatibility are consistent with what has been reported for the ADs *in vitro*, e.g., for embryonic kidney cells (HEK 293), and *in vivo*, namely in mice [31,44,45], while also presenting favourable safety profiles for all AD-NAM formulations.

Overall, this evaluation led to two main conclusions: i) the clinical isolate presents phenotypic differences that partially challenge the AD-NAM strategy, namely when using 1a; however, 1b-PNA continues to exert significant antibacterial activity, and ii) no toxicity was associated with the compounds under study (at the concentrations in use). For future studies, an antibacterial assessment using relevant *in vivo* models should be considered, to further validate the clinical translation of this strategy.

3. Conclusion

Antimicrobial resistance poses a growing threat to public health by rendering traditional antibiotics obsolete, underscoring the urgent need for innovative antibacterial agents. Antisense oligonucleotides present a promising alternative, by targeting and inhibiting specific bacterial genes, providing a novel approach to combating resistant pathogens. However, the multi-layered bacterial envelope is impermeable to these oligonucleotides, even those composed of nucleic acid mimics (that provide increased bio-stability and target affinity). To address this challenge, our group innovatively proposed a combined formulation of amphiphilic dendrimers and NAM-based oligos (targeting the *acpP* essential gene) against *E. coli*.

This study demonstrated that the amphiphilic dendrimers bearing primary and tertiary amine terminals, 1a and 1b, promote envelope permeabilisation of *E. coli*, as evidenced through i) PI internalisation detected via flow cytometry and ii) structural changes observed in the envelope using TEM. Furthermore, the combination of NAM-based oligos with both ADs enhanced NAM internalisation, as confirmed by the fluorescence detection of Cy3-labelled NAMs using both flow cytometry and epifluorescence microscopy. Ultimately, the AD-NAM formulations displayed effective antibacterial properties against *E. coli*, as evaluated using both a reference strain and a clinically relevant strain. Among the tested formulations, those with 1b led to the most significant reduction in bacterial counts, likely due to its inherent enhanced potency compared to 1a. Regarding NAM chemistry, the formulations with the PNA-based NAM emerged as the most effective, resulting in very substantial reductions of bacterial load (of up to 8 $\log_{10}$ CFU/mL), with sustained activity up to 24 h. Of particular interest is the specificity of the observed effect, as the PNA-based targeted NAM consistently outperformed the scrambled sequence of the same chemistry. This highlights the potential for designing pathogen-specific antibacterial drugs that effectively target harmful bacteria while preserving beneficial microbiota. By minimising off-target effects and disruption to the microbiome, these drugs also reduce the likelihood of resistance development when compared to traditional antibiotics. Finally, the tested formulations showed no signs of toxicity in *G. mellonella*, confirming their safety in an animal model.

These results highlight, for the first time, the potential of the antisense NAM strategy when combined with amphiphilic dendrimer vectors, and motivate our group to pursue additional studies towards optimisation and validation of clinical translation. Therefore, future work will focus on exploring antisense specificity by testing these formulations in complex biofilms, and conducting comprehensive *in vivo* studies to confirm their therapeutic potential.

4. Materials and methods

4.1. Amphiphilic dendrimers (ADs)

The amphiphilic dendrimers 1a and 1b were obtained via the ongoing collaboration with Dr. Ling Peng, from the Interdisciplinary Center of Nanoscience of Marseille (CINaM), and are further described in Dhumal *et al.* [31,32] Shortly, these two ADs, represented in Fig. 1A and described in Table 2, are composed of a long hydrophobic alkyl chain and a hydrophilic poly(amidoamine) (PAMAM) dendron, carrying a primary amine (1a) or a tertiary amine (1b), respectively. These ADs rely on dynamic self-assembling to form supramolecular structures when in solution.

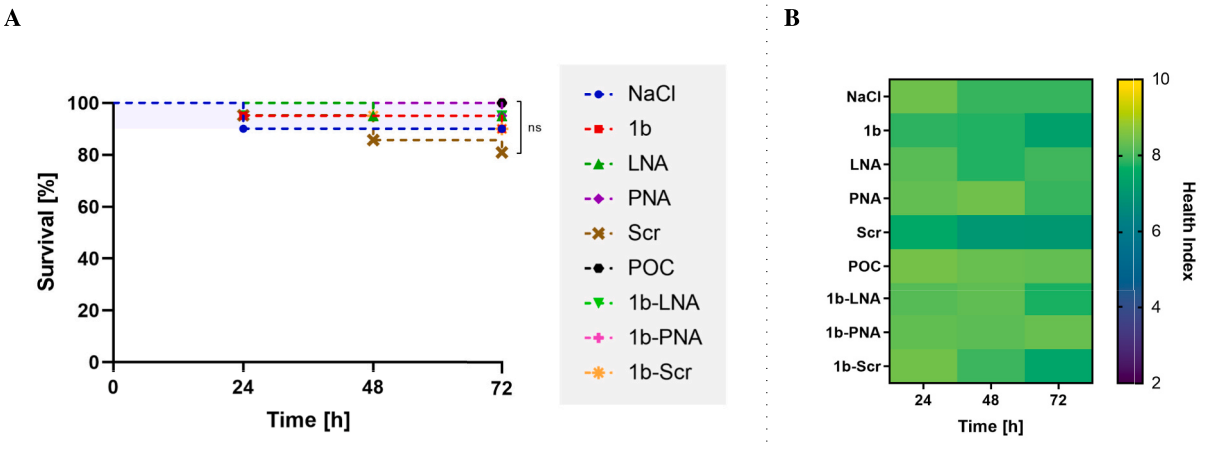

Fig. 10. Evaluation of the biocompatibility of the AD-NAMs and their components, as observed through **(A)** the survival and **(B)** health index of *G. mellonella* larvae over time. **(A and B)** Toxicity of the AD-NAM complexes, based on 1b, when combined with the LNA-based NAM (LNA), the PNA-based NAM (PNA), or the PNA-based scramble sequence (Scr). The peptide-oligonucleotide conjugate (POC) and the solo NAMs were also tested, and physiological saline (NaCl) was used as a control. The mean of at least two independent experiments is presented. Statistical differences, in comparison to NaCl, are indicated when appropriate in * ($p > 0.05$, ns). No toxicity was associated with the AD-NAM formulations or their solo components.

Table 2
Identification of the ADs used in this study.

ID	Description	Chemical formula
1a	Amphiphilic dendrimer in study, differentiated by its primary amine terminals	$C_{91}H_{182}N_{32}O_{14}$
1b	Amphiphilic dendrimer in study, differentiated by its tertiary amine terminals	$C_{107}H_{214}N_{32}O_{14}$

4.2. Nucleic acid mimics (NAMs)

The *acpP* gene in *E. coli* was selected as the antisense target for this study. This essential gene, which codes for a protein involved in fatty acid biosynthesis, is widely established as a target in bacterial antisense strategies [13–15]. Two different NAMs were synthesised: (i) an LNA/2′O-Me chimaera, and (ii) a PNA-based oligonucleotide, as clarified in Table 3. These sequences target the start codon region, based on prior studies [14,72]. Additionally, as a positive control, the PNA-based sequence was conjugated with the cell-penetrating peptide, $(KFF)_3K$. As a negative control, a scrambled sequence was designed by randomly rearranging the nucleotides of the PNA-based sequence. For fluorescence-based assays, the compounds were labelled at 5′ with Cy3. All NAM-based reagents were purchased from Eurogentec [Kaneca Eurogentec S.A.]. Low-retention pipette tips [AHN myTip LT 200 µL (Low Retention Tips), 4–121–50-0, AHN Biotechnologie GmbH] and low-binding microtubes [Low Protein Binding Microcentrifuge Tubes 1.5 mL, 90410, Thermo Scientific] were used when handling these compounds.

4.3. Preparation of AD-NAMs

Intermediate solutions of the studied ADs and NAMs were prepared in physiological saline (0.85 % NaCl) [Sodium Chloride, 7647-14-5, VWR International] or ultrapure water. To promote complexation (as adapted from Chen *et al.* [30]), equal volumes of these solutions were mixed, adding the AD solution to the NAM solution, and incubating the mix for 30 min at 37 °C [Refrigerated incubator FOC 225E, VELP Scientifica]. The resulting complexes, herein entitled AD-NAMs, are characterised by a Nitrogen/Phosphate (N/P) ratio. This value can be determined according to Eq. 1, in which C_{AD} and C_{NAM} are, respectively, the concentrations of the AD and NAM; N_{AD} is the number of amine terminal groups in the AD (8 for both 1a and 1b); and N_{NAM} is the number of monomers of the NAM sequence (10 for the selected sequences). Throughout this study, an N/P ratio of 1 was selected for all formulations. Therefore, the selected AD-NAM formulations included AD at MIC_{80} (18.8 µM) and NAMs at 15.0 µM.

$$\frac{N}{P} = \frac{C_{AD} \times N_{AD}}{C_{NAM} \times N_{NAM}} \quad (1)$$

Table 3
Identification of the antisense NAMs used in this study. Legend: "{}" – LNA monomers; "[]" – 2′O-Me monomers.

ID	Description	Sequence (5′-3′)
LNA	LNA/2′O-Me chimaera, targeting the *acpP* gene	{G}[C][U]{C}[A][U]{A}[C]{T}[C]
PNA	PNA-based oligonucleotide, targeting the *acpP* gene	GCTCATACTC
POC	Peptide-oligo conjugate, used as a positive control	GCTCATACTC–KFFKFFKFFK
P	Cell-penetrating peptide	KFFKFFKFFKK
Scr	Scrambled PNA-based sequence	ATCCTAGTCC

4.4. AD and AD-NAM characterisation

4.4.1. Transmission electron microscopy (TEM) - negative staining

Micrographs were obtained to visualise the supramolecular structures formed by the ADs and AD-NAMs when in solution. In short, the selected formulations were prepared in ultrapure water at the effective concentration of use (18.8 µM for ADs and 15.0 µM for NAMs). An aliquot (5 µL) was deposited onto a 300 mesh copper grid [Gilder grids, DG300-Cu, Delta Microscoscopy] and left to absorb for 10 min at room temperature in the dark. The grid was then stained with 1 % uranyl acetate (5 µL) [Uranyl Acetate, 22400, Electron Microscopy Sciences] for 1 min, and any excess liquid was removed using blotting paper before the measurements. Visualisation was performed at 80 kV in a transmission electron microscope [JEM 1400 Electron Microscope, JEOL] and digital images were acquired using an appropriate camera [PHURONA Camera, EMSIS GmbH]. Acquired images were analysed using Fiji (ImageJ, open platform for scientific image analysis) [73]. For each sample, at least 12 images (at magnifications ranging from 25000 × to 120000 ×) were analysed using a semi-automated segmentation method (Fig. A.3 in Supplementary Data). This method relied on applying an appropriate (user-selected) bandpass filter and automated thresholding for particle segmentation. Afterwards, binary tools (such as Fill Holes and Watershed) were used to approximate the mask to the detected particles. Lastly, particles were analysed, restraining circularity to 0.50–1.00 and excluding those with an area smaller than 5 nm^2. Throughout this study, particle size was reported as the mean and standard deviation of the obtained Feret diameter measurements.

4.4.2. Electrophoretic light scattering (ELS)

The zeta potential of each of the ADs and their resulting complexes with LNA and PNA was assessed via ELS measurements in low-salt aqueous solution (10 mM NaCl) at 25 °C. Measurements were performed using disposable cuvettes [Folded capillary zeta cell DTS1070, Malvern Panalytical] in an appropriate apparatus [Zetasizer Nano ZS, Malvern Panalytical].

4.4.3. Size exclusion chromatography (SEC)

The loading efficiency was used to characterise the success of the interaction between ADs and NAMs. The results were derived from fluorescence measurements, comparing the formulations of ADs with Cy3-labelled NAMs before and after appropriate partitioning from the non-complexed NAMs. The selected formulations were prepared in ultrapure water at the effective concentration of use (18.8 µM for ADs and 15.0 µM for Cy3-labelled NAMs). Upon mixing and the usual 30 min of incubation, an original aliquot (60 µL) was kept for fluorescence measurements, defining the total NAM fluorescence, i.e., when all NAMs are available in the solution ($F_{Total\ NAMs}$). Non-complexed NAMs were removed by passing an aliquot of the original formulation through a size exclusion chromatography column [PD SpinTrap™ G-25, 28–9180-04, Cytiva], following the protocol suggested in the columns' manual [74]. In short, spin columns were prepared, and the storage solution was removed by centrifugation for 1 min at 800 rcf. For equilibration, 400 µL of ultrapure water were added to each column, followed by centrifugation for 1 min at 800 rcf and rejection of the flow-through. This process was repeated 5 × in total. An aliquot (140 µL) of the AD-NAM mixture was then added to the columns and eluted into a clean collection tube by centrifugation (2 min at 800 rcf). This procedure was repeated at selected time points (0, 2, 4, 6, 8 and 24 h) to assess AD-NAM stability and release. An aliquot (60 µL) of each of the eluted solutions was kept for fluorescence measurements, defining the loaded NAM fluorescence at each time, i.e., that of NAMs that maintained interaction with the ADs ($F_{Loaded\ NAMs}$). All fluorescent aliquots were added to a black 96-well plate [Nunc™ 96-well polypropylene sample processing & storage microplates, 249945, Thermo Scientific™] and measured using a fluorescence microplate reader [FLUOstar Omega, BMG LABTECH], equipped with an appropriate filter (Excitation: 560–10; Emission:

600–10). The loading efficiency (*LE*) was calculated as described in Eq. 2.

$$LE[\%] = \frac{F_{\text{Loaded NAMs}}}{F_{\text{Total NAMs}}} \times 100 \quad (2)$$

4.5. Bacterial strains and growth conditions

E. coli was the main focus of this study. Strain ATCC 25922 was selected and used for the majority of the in vitro assays, given its ease of use and availability in most laboratories. As a pathogenic representative of this species, isolate H26 (U78734) was used as a more clinically relevant strain. Additionally, to assess the range of effect of the ADs, some assays included the use of *Bacillus subtilis* ATCC 6051 and *Staphylococcus epidermidis* ATCC 35984. These strains are summarised in Table 4.

To prepare an inoculum, the selected strain was grown overnight in tryptic soy broth (TSB) [Tryptic Soy Broth, 105459, Millipore] at 37 °C with shaking (160 rpm) [KS 130 Basic orbital shaker, IKA]. To obtain colony forming units (CFUs) and allow its enumeration, the bacteria were grown in its agar-supplemented (15 % *v*/v) counterpart, tryptic soy agar (TSA) [Agar powder, 9002-18-0, VWR International].

4.6. Bacterial susceptibility assays

The monitoring of growth was used to evaluate the antibacterial effect of the selected formulations. Two distinct methods were used for this analysis:

4.6.1. Turbidity reduction assay (TRA)

For a quick and high throughput analysis, a spectrophotometry-based assay was employed, adapted from Motyl *et al.* [79] and Wiegand *et al.* [80] An overnight culture of the selected strain was diluted to 2 × 6 $\log_{10}$ CFU/mL (OD_{600nm} of 0.01 for *E. coli*) in concentrated MHB (x2) [Mueller Hinton Broth, 70192, Millipore]. Alternatively, LB-Miller (x2) [LB Broth, Miller (Luria-Bertani), 97064–110, VWR] was used during a preliminary media study. This cell suspension (100 μL) was added to the wells of a sterile 96-well plate [Tissue Culture Plate, 734–2327, VWR] and incubated with different formulations of the tested compounds (100 μL) at 37 °C. This resulted in a bacterial concentration of approximately 6 $\log_{10}$ CFU/mL for all samples. The OD_{600nm} was monitored for 24 h using a plate reader [Spectrostar Nano, BMG Labtech], with absorbance measurements every 30 min (total of 49 cycles), for all used wells (200 μL/well). An orbital shaking was defined with a frequency of 200 rpm for 100 s before each measurement cycle. Besides the tested formulations, each tested plate included controls for the medium, ensuring sterility (SC), and bacterial growth (GC).

The minimum inhibitory concentration (MIC) was objectively defined as the lowest concentration that led to a reduction of at least 80 % in growth (MIC_{80}), as detected through the measurement of OD_{600nm}, when compared to the growth control [81,82]. Additionally, the minimum bactericidal concentration (MBC) was determined by sub-culturing aliquots, obtained from all wells that showed no visible microbial growth, on the surface of TSA plates and determining the number of surviving cells (in CFU/mL) after a 24 h incubation at 37 °C. The MBC was defined as the lowest concentration of the antibacterial agent needed to kill 99.9 % of the inoculum [81,82]. Throughout this study, the overall variation of the MICs/MBCs was presented using the individual values obtained for independent experiments. The effective MIC/MBC values were then determined based on the consistency of the results (represented by the median).

Table 4
List of bacterial strains selected for the study. Abbreviations: ATCC, American Type Culture Collection; CLSI, Clinical and Laboratory Standards Institute.

Bacterial strain	Relevant characteristics	Source
Escherichia coli ATCC 25922	CLSI control strain for antimicrobial susceptibility testing; common lab strain; biotype 1.	[75,76]
Escherichia coli H26 (U78734)	Isolate from haemoculture (Oct 2017); multi-resistant isolate (more information in Table A.2 in Supplementary data); biotype 2.	–
Bacillus subtilis ATCC 6051	Type strain; application in quality control and resistance testing; biotype 1.	[77]
Staphylococcus epidermidis ATCC 35984	Genome sequenced strain originally isolated from a case of catheter sepsis; biotype 1.	[78]

4.6.2. Time-kill assay (TKA)

For a more thorough analysis, a CFU-based assay was employed, to determine the evolution of viable (and culturable) cells over time. A bacterial suspension, prepared similarly to what was described for TRA, was incubated with the selected formulations for 24 h at 37 °C. Instead of OD monitoring, this assay relied on the sampling (10 μL) and microdilution of all test samples, at selected time points (0, 2, 4, 6, 8 and 24 h). Besides the tested formulations, each experiment included controls for the medium, ensuring sterility (SC), and normal bacterial growth (UnEC). Appropriate dilutions were plated in order to determine the number of surviving cells (in CFU/mL), using the track dilution method [79,83]. The evolution of CFU/mL of each sample throughout time was then plotted, clarifying the antibacterial profile of each formulation. The detection limit was calculated assuming a single colony forming unit (CFU) is the smallest amount quantifiable from a 10 μL aliquot of the original sample (dilution factor of 1). The concentration of surviving cells is determined using Eq. 3, for which *C* is the number of bacterial colonies, *D* is the dilution factor and *V* is the volume of the aliquot.

$$\begin{aligned} \text{Measure of surviving cells} &= \frac{C}{D \times V} = \frac{\text{CFU}}{\text{mL}} \\ \Rightarrow \text{Limit of detection} &= \frac{1\ \text{CFU}}{1 \times 0.01\ \text{mL}} = 10^2\ \frac{\text{CFU}}{\text{mL}} \end{aligned} \quad (3)$$

This results in a detection limit of 10^2 CFU/mL, as represented in the graphs. However, there are cases in which no CFUs were detected after treatment. For simplicity's sake, those situations were represented as ∼ 0 CFU/mL.

4.7. Evaluation of membrane permeabilisation

4.7.1. Flow cytometry with propidium iodide stain

The permeabilisation caused to the envelope by the ADs was assessed using propidium iodide (PI) [LIVE/DEAD® BacLight™ Bacterial Viability Kit, L7012, Invitrogen]. This dye is a red-fluorescent nucleic acid stain, which only penetrates bacteria with compromised membranes [84].

This PI-based membrane integrity assay was previously optimised in-house. An incubation time of 15 min was selected to minimise the overlap of unviable vs permeabilised bacterial populations. In short, an overnight inoculum was diluted to obtain an OD_{600nm} of 0.01. The resulting bacterial suspension (100 μL) was then centrifuged for 5 min at 10000 rcf [Centrifuge 5418, Eppendorf]. After removing the supernatant, the bacterial pellet was resuspended in a saline-based solution (200 μL) of the constructs (at the final concentration of study). The mixture was incubated for 15 min at 37 °C, and, once again, centrifuged for 5 min at 10000 rcf. The bacterial cells were resuspended in PI (50 μL, 7.4 μM), and incubated for 4 min. After another centrifugation, the bacterial cells were washed in 1 mL of ultrapure water. A last centrifugation was performed before resuspending the pellet in ultrapure water. Polymyxin (15 min at MIC_{80}, 2.5 μg/mL) [Polymyxin B sulfate salt, P1004-1MU, Sigma-Aldrich] and ethanol (30 min at 50 %) [Ethanol 70 % (*v*/v) TechniSolv, 83801.360, VWR Chemicals] were used as positive controls.

The resulting samples were analysed using a cytometer equipped with a 488 nm laser [CytoFLEX Flow Cytometer, V0-B3-R1, Beckman Coulter]. Parameters such as the forward angle light scatter (FS), side angle light scatter (SS) and red fluorescence (using the PC5.5 filter) were detected with a minimum of 30000 events falling into the defined bacterial gate (on the FS-SS plot). The data was analysed via the equipment's software [CytExpert, Beckman Coulter], and the average percentage of PI-positive bacteria was determined for each experiment.

4.7.2. Transmission electron microscopy (TEM) - chemical fixation

Micrographs were obtained to visualise the changes caused by the ADs to the bacterial envelope of *E. coli* and its surroundings. In short, an overnight inoculum was diluted to obtain an OD_{600nm} of 0.01 in MHB (x2). This cell suspension (100 μL) was incubated with the selected formulations (100 μL) at 37 °C. In order to guarantee enough changes could be detected, samples with the ADs were incubated for 2 h; in order to avoid bacterial loss, samples with polymyxin were incubated for 15 min only. The samples were fixed for 2 h (minimum) at 4 °C in an equal volume (200 μL) of 5 % glutaraldehyde [Aqueous Glutaraldehyde EM Grade 50 %, 16316, Electron Microscopy Sciences] and 4 % paraformaldehyde [Paraformaldehyde 20 % Aqueous Solution EM Grade, 15713, Electron Microscopy Sciences] in 0.2 M sodium cacodylate buffer [Trihydrate Sodium Cacodylate, 12300, Electron Microscopy Sciences], followed by 3 washings in buffer, 5 min each. The resulting pellets were embedded in processing gel [HistoGel™, HG-400-012, Thermo Scientific™]. The samples were then postfixed for 2 h in 2 % osmium tetroxide [Osmium Tetroxide 4 % Aqueous Solution, 19190; Electron Microscopy Sciences] in 0.1 M sodium cacodylate buffer. After being washed in water (3 × , 5 min each), samples were stained for 30 min with 1 % uranyl acetate [Uranyl Acetate, 22400, Electron Microscopy Sciences]. After another wash in distilled water, the samples were immersed in an ethanol series (50 %, 70 %, 80 %, 100 %, 100 %, 100 %) followed by propylene oxide (PO), for dehydration [Propylene Oxide, 20401, Electron Microscopy Sciences]. The samples were then embedded in EMbed 812 resin through a gradient of PO:resin [EMbed 812 Kit for Electron Microscopy Embedding, 14120, Electron Microscopy Sciences]. The infiltrations were performed for at least 1 h in a 3:1 solution, followed by a 1:1 of the same reagents overnight, and a 1:3 solution for 1 h. Finally, samples were embedded in the resin and ready for cutting. Ultrathin sections (50 nm) were cut using a diamond knife on an ultramicrotome [PowerTome PT XL, RMC Boeckeler], mounted on 300 mesh copper grids [Gilder grids, DG300-Cu, Delta Microscoscopy], and contrasted with uranyl acetate substitute [Uranyl Acetate Substitute, 11000, Electron Microscopy Sciences] and lead citrate [Lead Citrate, 11300, Electron Microscopy Sciences]. For samples incubated with 1a and 1b, there was a noticeable loss of bacterial cells, culminating in the difficult processing of the TEM resin blocks. Nonetheless, the remaining cells allowed representative visualisation. Visualisation was performed at 80 kV in a transmission electron microscope [JEM 1400 Electron Microscope, JEOL] and digital images were acquired using an appropriate camera [PHURONA Camera, EMSIS GmbH].

4.8. Evaluation of the internalisation of NAMs

4.8.1. Epifluorescence microscopy

The internalisation in bacteria of the Cy3-labelled NAMs was assessed using a fluorescence in situ hybridisation (FISH)-based assay. However, this protocol did not include the traditional bacterial fixation and permeabilisation, as the ADs are expected to replace the need for toxic permeabilisation/fixation agents [85,86]. This assay was performed as described by Pereira *et al* [24], with some modifications.

In short, an overnight inoculum was diluted to obtain an OD_{600nm} of 0.01 in saline. The resulting bacterial suspension (100 μL) was mixed with an equal volume of the fluorescently labelled constructs. The mixture was incubated for 15 min at 37 °C and later centrifuged for 10 min at 16400 rcf. The bacterial cells were then washed in 500 μL of washing solution (0.005 M Tris base [Tris Base, 77–86-1, Fisher Scientific], 0.015 M NaCl, 0.1 % v/v Triton-X [Triton X-100, Panreac], pH 10) for 15 min, at 37 °C. After another centrifugation (10 min at 16400 rcf) and removal of the supernatant, the bacterial cells were resuspended in sterile ultrapure water (100 μL), and 20 μL of each sample were placed on a glass slide well and dried at 37 °C. Once dry, the samples were ready for in-slide bacterial staining. As such, 20 μL of DAPI (0.1 mg/mL) [4′,6′-diamidino-2-phenylindole dihydrochloride, 28718–90-3, Merck] were added to each well and incubated for 10 min, followed by a washing with ultrapure water. After drying, the samples were visualised on an epifluorescence microscope [Eclipse Ti-SR inverted microscope, Nikon] using a 100 × oil objective [CFI Plan Apo λ 100 × /1.45NA Oil, Nikon] and a G-2A longpass filter (excitation: 535–50 nm; emission: 580 nm) for orange fluorescence or a DAPI bandpass filter (excitation: 375–28 nm; emission: 460–60 nm) for blue fluorescence. At least five fields of view of each sample were taken using a monochromatic camera [QImaging Retiga R1, Cairn Research] and processed using appropriate software [IS-Elements Advanced Research, Nikon]. The exposure time and excitation intensity were maintained throughout the experiments. Acquired images were analysed using Fiji (ImageJ, open platform for scientific image analysis) [73].

4.8.2. Flow cytometry

Flow cytometry was implemented not only to show the membrane damage but also to further quantify the internalisation of NAMs in *E. coli*. Samples were prepared in a similar manner to that executed for the epifluorescence microscopy studies (up to resuspension in ultrapure water).

The resulting samples were analysed using the aforementioned cytometer. Parameters such as the forward angle light scatter (FS), side angle light scatter (SS) and orange fluorescence (using the PE filter) were detected with a minimum of 30000 events falling into the defined bacterial gate (on the FS-SS plot). The data was analysed via the equipment's software, and the average percentage of Cy3-positive bacteria as well as the median of a sample's fluorescence intensity was determined for each experiment.

4.9. In vivo studies – Galleria mellonella model

Galleria mellonella was used as the model host to determine the toxicity associated with the proposed formulations. Based on the protocol described by Araújo *et al.* [87], *G. mellonella* larvae were reared at 25 °C, in darkness, with a pollen grain diet [Pólen Seco, Nuno Marques – Comércio de Mel, Lda., Mértola]. The caterpillars were used at their last larval stage, with a weight of approximately 250 mg. The larvae were injected via the hindmost left proleg, previously cleansed with 70 % (*v*/v) ethanol, using an insulin syringe [BD Micro Fine, Frilabo], to control the volume of injection (10 μL) and to reach the haemolymph (intra-haemocoelic injection). For each condition, at least 10 larvae were injected with the respective formulation. Afterwards, all larvae were stored in the dark at 37 °C.

Larvae's health and survival were monitored and registered up to 72 h (in 24 h intervals), using a standardised scoring system (proposed by Loh *et al.* [88] and illustrated by Tsai *et al.* [89]). Their health index was calculated based on four main parameters: (i) larvae activity, (ii) cocoon formation, (iii) melanisation, and (iv) survival. The larvae were considered dead when they displayed no movement in response to touch.

To evaluate the toxicity associated with the AD-NAM formulations, the *G. mellonella* larvae were injected with a saline-based solution of the AD-NAMs in study, as well as their solo counterparts (ADs or NAMs alone). As a negative control, a set of larvae were injected with saline only.

4.10. Statistical analysis

The software GraphPad Prism [v8.4.0, GraphPad Software] was used for statistical analysis. Experiments were performed in triplicates (minimum) on independent days. Descriptive statistics used throughout the text relate to the average values and standard deviation of the sampled groups. Given the need to compare several formulations, the significance between the means of the experimental groups was evaluated using one-way analysis of variance (ANOVA). Each of these analyses was followed by Tukey's multiple-comparison test. A p-value of $\leq$ 0.05 (95 % confidence interval) was considered as significant ($p > 0.05$, ns; $p \leq 0.05$, *; $p \leq 0.01$, **; $p \leq 0.001$, ***; $p \leq 0.0001$, ****). For further comparison between groups, regarding NAM internalisation, a two-way ANOVA analysis was performed. Additionally, for the evaluation of *G. mellonella* survival, Kaplan-Meier curves were plotted and differences in survival were calculated using the log-rank (Mantel-Cox) statistical test.

4.11. Figures

Drawings of chemical structures were produced using MarvinSketch [v23.17, 2023, ChemAxon]. Graphical representations, such as plots and heatmaps, were produced using GraphPad Prism [v8.4.0, GraphPad Software]. Microscopy images were analysed and edited using Fiji (ImageJ, open platform for scientific image analysis) [73]. Lastly, vector-based figures, such as the graphical abstract, were produced using Inkscape [v1.3.2, 2023, Inkscape Developers].

CRediT authorship contribution statement

Mariana Gomes: Writing – review & editing, Writing – original draft, Visualisation, Methodology, Investigation, Formal analysis, Conceptualization. **Igor Resende:** Writing – review & editing, Investigation, Conceptualization. **Yana Zamoshchak:** Investigation. **Daniela Araújo:** Writing – review & editing, Resources, Investigation. **Joana Castro:** Writing – review & editing, Investigation. **Dinesh Dhumal:** Resources. **Ling Peng:** Writing – review & editing, Resources. **Rita S. Santos:** Writing – review & editing, Supervision, Project administration, Methodology, Conceptualization. **Nuno F. Azevedo:** Writing – review & editing, Supervision, Project administration, Funding acquisition, Conceptualization.

Declaration of generative AI and AI-assisted technologies in the writing process

During the preparation of this manuscript, the authors used Microsoft's Copilot and OpenAI's ChatGPT in order to improve spelling, grammar and readability. After using these tools, the authors reviewed and edited the content as needed and take full responsibility for the content of the publication.

Funding

This work was financially supported by: (i) national funds through FCT/MCTES (PIDDAC): LEPABE, UIDB/00511/2020 (DOI: 10.54499/UIDB/00511/2020) and UIDP/00511/2020 (DOI: 10.54499/UIDP/00511/2020) and ALiCE, LA/P/0045/2020 (DOI:10.54499/LA/P/0045/2020); (ii) project DELNAM - European Union's Horizon 2020 research and innovation programme under grant agreement No. 810685; (iii) project e.Biofilm, financed by the European Commission in the scope of the Horizon Europe Framework Programme, under grant agreement No. 101087568; (iv) PhD grant No. 2022.10864.BD (DOI: 10.54499/2022.10864.BD), funded by national funds through Fundação para a Ciência e a Tecnologia (FCT); and (v) CEEC Individual contracts (DOI: 10.54499/2022.06886.CEECIND/CP1737/CT0001 and DOI: 10.54499/2023.06040.CEECIND/CP2873/CT0001) funded by national funds through FCT.

Declaration of competing interest

The authors declare that they have no known competing financial interests or personal relationships that could have appeared to influence the work reported in this paper.

Acknowledgements

The amphiphilic dendrimers 1a and 1b were kindly provided by Dr Ling Peng and Dinesh Dhumal, from the Interdisciplinary Center of Nanoscience of Marseille (CINaM). The *E. coli* H26 isolate was kindly provided by Dr Daniela Araújo, from the Portuguese National Institute of Agrarian and Veterinary Research (INIAV). The TEM assays were performed in collaboration with Dr Rui Fernandes and Sofia Pacheco, at the HEMS Core Facility in the Institute of Health Innovation and Research (I3S) from the University of Porto. The ELS measurements were performed at the Laboratory of Separation and Reaction Engineering and Laboratory of Catalysis and Materials (LSRE-LCM) in FEUP, with access kindly provided by Dr Yaidelin Manrique. Special thanks to João Santos for sharing his know-how on SEC and providing reagents for the preliminary testing. Special thanks to Dr Darla Goeres for reviewing the manuscript and providing valuable feedback as a native speaker.

Appendix A. Supplementary data

Supplementary data to this article can be found online at https://doi.org/10.1016/j.jconrel.2025.113850.

Data availability

Data will be made available on request.

References

[1] European Centre for Disease Prevention and Control (ECDC), 35 000 annual deaths from antimicrobial resistance in the EU/EEA, URL: https://www.ecdc.europa.eu/en/news-events/eaad-2022-launch, 2022.
[2] WHO Regional Office for Europe, European Centre for Disease Prevention and Control (ECDC), Antimicrobial resistance surveillance in Europe 2022–2020 data, Technical Report, 2022.
[3] M. Naghavi, S.E. Vollset, K.S. Ikuta, L.R. Swetschinski, A.P. Gray, E.E. Wool, G. Robles Aguilar, T. Mestrovic, G. Smith, C. Han, R.L. Hsu, J. Chalek, D.T. Araki, E. Chung, C. Raggi, A. Gershberg Hayoon, N. Davis Weaver, P.A. Lindstedt, A. E. Smith, U. Altay, N.V. Bhattacharjee, K. Giannakis, F. Fell, B. McManigal, N. Ekapirat, J.A. Mendes, T. Runghien, O. Srimokla, A. Abdelkader, S. Abd-Elsalam, R.G. Aboagye, H. Abolhassani, H. Abualruz, U. Abubakar, H. J. Abukhadijah, S. Aburuz, A. Abu-Zaid, S. Achalapong, I.Y. Addo, V. Adekanmbi, T.E. Adeyeoluwa, Q.E.S. Adnani, L.A. Adzigbli, M.S. Afzal, S. Afzal, A. Agodi, A. J. Ahlstrom, A. Ahmad, S. Ahmad, T. Ahmad, A. Ahmadi, A. Ahmed, H. Ahmed, I. Ahmed, M. Ahmed, S. Ahmed, S.A. Ahmed, M.A. Akkaif, S. Al Awaidy, Y. Al Thaher, S.O. Alalalmeh, M.T. AlBataineh, W.A. Aldhaleei, A.A.S. Al-Gheethi, N. B. Alhaji, A. Ali, L. Ali, S.S. Ali, W. Ali, K. Allel, S. Al-Marwani, A. Alrawashdeh, A. Altaf, A.B. Al-Tammemi, J.A. Al-Tawfiq, K.H. Alzoubi, W.A. Al-Zyoud, B. Amos, J.H. Amuasi, R. Ancuceanu, J.R. Andrews, A. Anil, I.A. Anuoluwa, S. Anvari, A. E. Anyasodor, G.L.C. Apostol, J. Arabloo, M. Arafat, A.Y. Aravkin, D. Areda, A. Aremu, A.A. Artamonov, E.A. Ashley, M.O. Asika, S.S. Athari, M.M.W. Atout, T. Awoke, S. Azadnajafabad, J.M. Azam, S. Aziz, A.Y. Azzam, M. Babaei, F.-X. Babin, M. Badar, A.A. Baig, M. Bajcetic, S. Baker, M. Bardhan, H.J. Barqawi, Z. Basharat, A. Basiru, M. Bastard, S. Basu, N.S. Bayleyegn, M.A. Belete, O.O. Bello, A. Beloukas, J.A. Berkley, A.S. Bhagavathula, S. Bhaskar, S.S. Bhuyan, J.A. Bielicki, N.I. Briko, C.S. Brown, A.J. Browne, D. Buonsenso, Y. Bustanji, C.G. Carvalheiro, C. A. Castañeda-Orjuela, M. Cenderadewi, J. Chadwick, S. Chakraborty, R. M. Chandika, S. Chandy, V. Chansamouth, V.K. Chattu, A.A. Chaudhary, P. R. Ching, H. Chopra, F.R. Chowdhury, D.-T. Chu, M. Chutiyami, N. Cruz-Martins, A.G. da Silva, O. Dadras, X. Dai, S.D. Darcho, S. Das, F.P. De la Hoz, D.M. Dekker, K. Dhama, D. Diaz, B.F.R. Dickson, S.G. Djorie, M. Dodangeh, S. Dohare, K. G. Dokova, O.P. Doshi, R.K. Dowou, H.L. Dsouza, S.J. Dunachie, A.M. Dziedzic, T. Eckmanns, A. Ed-Dra, A. Eftekharimehrabad, T.C. Ekundayo, I. El Sayed, M. Elhadi, W. El-Huneidi, C. Elias, S.J. Ellis, R. Elsheikh, I. Elsohaby, C. Eltaha, B. Eshrati, M. Eslami, D.W. Eyre, A.O. Fadaka, A.F. Fagbamigbe, A. Fahim, A. Fakhri-Demeshghieh, F.O. Fasina, M.M. Fasina, A. Fatehizadeh, N.A. Feasey, A. Feizkhah, G. Fekadu, F. Fischer, I. Fitriana, K.M. Forrest, C. Fortuna Rodrigues, J.E. Fuller, M.A. Gadanya, M. Gajdács, A.P. Gandhi, E.E. Garcia-Gallo, D.O. Garrett,

R.K. Gautam, M.W. Gebregergis, M. Gebrehiwot, T.G. Gebremeskel, C. Geffers, L. Georgalis, R.M. Ghazy, M. Golechha, D. Golinelli, M. Gordon, S. Gulati, R. D. Gupta, S. Gupta, V.K. Gupta, A.D. Habteyohannes, S. Haller, H. Harapan, M. L. Harrison, A.I. Hasaballah, I. Hasan, R.S. Hasan, H. Hasani, A.H. Haselbeck, M. S. Hasnain, I.I. Hassan, S. Hassan, M.S. Hassan Zadeh Tabatabaei, K. Hayat, J. He, O.E. Hegazi, M. Heidari, K. Hezam, R. Holla, M. Holm, H. Hopkins, M.M. Hossain, M. Hosseinzadeh, S. Hostiuc, N.R. Hussein, L.D. Huy, E.D. Ibáñez-Prada, A. Ikiroma, I.M. Ilic, S.M.S. Islam, F. Ismail, N.E. Ismail, C.D. Iwu, C.J. Iwu-Jaja, A. Jafarzadeh, F. Jaiteh, R. Jalilzadeh Yengejeh, R.D.G. Jamora, J. Javidnia, T. Jawaid, A.W.J. Jenney, H.J. Jeon, M. Jokar, N. Jomehzadeh, T. Joo, N. Joseph, Z. Kamal, K.K. Kanmodi, R.S. Kantar, J.A. Kapisi, I.M. Karaye, Y.S. Khader, H. Khajuria, N. Khalid, F. Khamesipour, A. Khan, M.J. Khan, M.T. Khan, V. Khanal, F.F. Khidri, J. Khubchandani, S. Khusuwan, M.S. Kim, A. Kisa, V.A. Korshunov, F. Krapp, R. Krumkamp, M. Kuddus, M. Kulimbet, D. Kumar, E.A.P. Kumaran, A. Kuttikkattu, H.H. Kyu, I. Landires, B.K. Lawal, T.T.T. Le, I.M. Lederer, M. Lee, S. W. Lee, A. Lepape, T.L. Lerango, V.S. Ligade, C. Lim, S.S. Lim, L.W. Limenh, C. Liu, X. Liu, X. Liu, M.J. Loftus, H.I.M. Amin, K.L. Maass, S.B. Maharaj, M.A. Mahmoud, P. Maikanti-Charalampous, O.M. Makram, K. Malhotra, A.A. Malik, G. D. Mandilara, F. Marks, B.A. Martinez-Guerra, M. Martorell, H. Masoumi-Asl, A. G. Mathioudakis, J. May, T.A. McHugh, J. Meiring, H.N. Meles, A. Melese, E. B. Melese, G. Minervini, N.S. Mohamed, S. Mohammed, S. Mohan, A.H. Mokdad, L. Monasta, A. Moodi Ghalibaf, C.E. Moore, Y. Moradi, E. Mossialos, V. Mougin, G. D. Mukoro, F. Mulita, B. Muller-Pebody, E. Murillo-Zamora, S. Musa, P. Musicha, L. A. Musila, S. Muthupandian, A.J. Nagarajan, P. Naghavi, F. Nainu, T.S. Nair, H.H. R. Najmuldeen, Z.S. Natto, J. Nauman, B.P. Nayak, G.T. Nchanji, P. Ndishimye, I. Negoi, R.I. Negoi, S.A. Nejadghaderi, Q.P. Nguyen, E.A. Noman, D.C. Nwakanma, S. O'Brien, T.J. Ochoa, I.A. Odetokun, O.A. Ogundijo, T.R. Ojo-Akosile, S.R. Okeke, O.C. Okonji, A.T. Olagunju, A. Olivas-Martinez, A.A. Olorukooba, P. Olwoch, K. I. Onyedibe, E. Ortiz-Brizuela, O. Osuolale, P. Ounchanum, O.T. Oyeyemi, M. P. P A, J.L. Paredes, R.R. Parikh, J. Patel, S. Patil, S. Pawar, A.Y. Peleg, P. Peprah, J. Perdigão, C. Perrone, I.-R. Petcu, K. Phommasone, Z.Z. Piracha, D. Poddighe, A. J. Pollard, R. Poluru, A. Ponce-De-Leon, J. Puvvula, F.N. Qamar, N.H. Qasim, C. D. Rafai, P. Raghav, L. Rahbarnia, F. Rahim, V. Rahimi-Movaghar, M. Rahman, M. A. Rahman, H. Ramadan, S.K. Ramasamy, P.S. Ramesh, P.W. Ramteke, R.K. Rana, U. Rani, M.-M. Rashidi, D. Rathish, S. Rattanavong, S. Rawaf, E.M.M. Redwan, L. F. Reyes, T. Roberts, J.V. Robotham, V.D. Rosenthal, A.G. Ross, N. Roy, K.E. Rudd, C.J. Sabet, B.A. Saddik, M.R. Saeb, U. Saeed, S. Saeedi Moghaddam, W. Saengchan, M. Safaei, A. Saghazadeh, N. Saheb Sharif-Askari, A. Sahebkar, S.S. Sahoo, M. Sahu, M. Saki, N. Salam, Z. Saleem, M.A. Saleh, Y.L. Samodra, A.M. Samy, A. Saravanan, M. Satpathy, A.E. Schumacher, M. Sedighi, S. Seekaew, M. Shafie, P. A. Shah, S. Shahid, M.J. Shahwan, S. Shakoor, N. Shalev, M.A. Shamim, M. A. Shamshirgaran, A. Shamsi, A. Sharifan, R.P. Shastry, M. Shetty, A. Shittu, S. Shrestha, E.E. Siddig, T. Sideroglou, J. Sifuentes-Osornio, L.M.L.R. Silva, E.A. F. Simões, A.J.H. Simpson, A. Singh, S. Singh, R. Sinto, S.S.M. Soliman, S. Soraneh, N. Stoesser, T.Z. Stoeva, C.K. Swain, L. Szarpak, S.S.T.Y.S. Tabatabai, C. Tabche, Z. M.-A. Taha, K.-K. Tan, N. Tasak, N.Y. Tat, A. Thaiprakong, P. Thangaraju, C. C. Tigoi, K. Tiwari, M.R. Tovani-Palone, T.H. Tran, M. Tumurkhuu, P. Turner, A. J. Udoakang, A. Udoh, N. Ullah, S. Ullah, A.G. Vaithinathan, M. Valenti, T. Vos, H. T.L. Vu, Y. Waheed, A.S. Walker, J.L. Walson, T. Wangrangsimakul, K. G. Weerakoon, H.F.L. Wertheim, P.C.M. Williams, A.A. Wolde, T.M. Wozniak, F. Wu, Z. Wu, M.K.K. Yadav, S. Yaghoubi, Z.S. Yahaya, A. Yarahmadi, S. Yezli, Y. E. Yismaw, D.K. Yon, C.-W. Yuan, H. Yusuf, F. Zakham, G. Zamagni, H. Zhang, Z.-J. Zhang, M. Zielińska, A. Zumla, S.H.H. Zyoud, S.H. Zyoud, S.I. Hay, A. Stergachis, B. Sartorius, B.S. Cooper, C. Dolecek, C.J.L. Murray, Global burden of bacterial antimicrobial resistance 1990–2021: a systematic analysis with forecasts to 2050, Lancet 404 (2024) 1199–1226, https://doi.org/10.1016/S0140-6736(24)01867-1.

[4] J.B. Kaper, J.P. Nataro, H.L.T. Mobley, Pathogenic *Escherichia coli*, Nat. Rev. Microbiol. 2 (2004) 123–140, https://doi.org/10.1038/nrmicro818.

[5] L.B. Rice, Federal funding for the study of antimicrobial resistance in nosocomial pathogens: no ESKAPE, J. Infect. Dis. 197 (2008) 1079–1081, https://doi.org/10.1086/533452.

[6] WHO, Prioritization of pathogens to guide discovery, research and development of new antibiotics for drug resistant bacterial infections, including tuberculosis, in: Technical Report, 2017.

[7] C.J.L. Murray, K.S. Ikuta, F. Sharara, L. Swetschinski, G.R. Aguilar, A. Gray, C. Han, C. Bisignano, P. Rao, E. Wool, S.C. Johnson, A.J. Browne, M.G. Chipeta, F. Fell, S. Hackett, G. Haines-Woodhouse, B.H.K. Hamadani, E.A.P. Kumaran, B. McManigal, S. Achalapong, R. Agarwal, S. Akech, S. Albertson, J. Amuasi, J. Andrews, A. Aravkin, E. Ashley, F.-X. Babin, F. Bailey, S. Baker, B. Basnyat, A. Bekker, R. Bender, J.A. Berkley, A. Bethou, J. Bielicki, S. Boonkasidecha, J. Bukosia, C. Carvalheiro, C. Castañeda-Orjuela, V. Chansamouth, S. Chaurasia, S. Chiurchiù, F. Chowdhury, R.C. Donatien, A.J. Cook, B. Cooper, T.R. Cressey, E. Criollo-Mora, M. Cunningham, S. Darboe, N.P.J. Day, M.D. Luca, K. Dokova, A. Dramowski, S.J. Dunachie, T.D. Bich, T. Eckmanns, D. Eibach, A. Emami, N. Feasey, N. Fisher-Pearson, K. Forrest, C. Garcia, D. Garrett, P. Gastmeier, A. Z. Giref, R.C. Greer, V. Gupta, S. Haller, A. Haselbeck, S.I. Hay, M. Holm, S. Hopkins, Y. Hsia, K.C. Iregbu, J. Jacobs, D. Jarovsky, F. Javanmardi, A.W. J. Jenney, M. Khorana, S. Khusuwan, N. Kissoon, E. Kobeissi, T. Kostyanev, F. Krapp, R. Krumkamp, A. Kumar, H.H. Kyu, C. Lim, K. Lim, D. Limmathurotsakul, M.J. Loftus, M. Lunn, J. Ma, A. Manoharan, F. Marks, J. May, M. Mayxay, N. Mturi, T. Munera-Huertas, P. Musicha, L.A. Musila, M.M. Mussi-Pinhata, R.N. Naidu, T. Nakamura, R. Nanavati, S. Nangia, P. Newton, C. Ngoun, A. Novotney, D. Nwakanma, C.W. Obiero, T.J. Ochoa, A. Olivas-Martinez, P. Olliaro, E. Ooko, E. Ortiz-Brizuela, P. Ounchanum, G.D. Pak, J.L. Paredes, A.Y. Peleg, C. Perrone, T. Phe, K. Phommasone, N. Plakkal, A.P. de Leon, M. Raad, T. Ramdin, S. Rattanavong, A. Riddell, T. Roberts, J.V. Robotham, A. Roca, V.D. Rosenthal, K. E. Rudd, N. Russell, H.S. Sader, W. Saengchan, J. Schnall, J.A.G. Scott, S. Seekaew, M. Sharland, M. Shivamallappa, J. Sifuentes-Osornio, A.J. Simpson, N. Steenkeste, A.J. Stewardson, T. Stoeva, N. Tasak, A. Thaiprakong, G. Thwaites, C. Tigoi, C. Turner, P. Turner, H.R. van Doorn, S. Velaphi, A. Vongpradith, M. Vongsouvath, H. Vu, T. Walsh, J.L. Walson, S. Waner, T. Wangrangsimakul, P. Wannapinij, T. Wozniak, T.E.M.W.Y. Sharma, K.C. Yu, P. Zheng, B. Sartorius, A.D. Lopez, A. Stergachis, C. Moore, C. Dolecek, M. Naghavi, Global burden of bacterial antimicrobial resistance in 2019: A systematic analysis, Lancet 399 (2022) 629–655, https://doi.org/10.1016/S0140-6736(21)02724-0.

[8] S. Tao, H. Chen, N. Li, T. Wang, W. Liang, The spread of antibiotic resistance genes *in vivo* model, Can. J. Infect. Dis. Med. Microbiol. 2022 (2022) 1–11, https://doi.org/10.1155/2022/3348695.

[9] S. Karkare, D. Bhatnagar, Promising nucleic acid analogs and mimics: characteristic features and applications of PNA, LNA, and morpholino, Appl. Microbiol. Biotechnol. 71 (2006) 575–586, https://doi.org/10.1007/s00253-006-0434-2.

[10] S. Bajan, G. Hutvagner, RNA-based therapeutics: from antisense oligonucleotides to miRNAs, Cells 9 (2020), https://doi.org/10.3390/cells9010137.

[11] R.S. Santos, C. Figueiredo, N.F. Azevedo, K. Braeckmans, S.C.D. Smedt, Nanomaterials and molecular transporters to overcome the bacterial envelope barrier: towards advanced delivery of antibiotics, Adv. Drug Deliv. Rev. 136-137 (2018) 28–48, https://doi.org/10.1016/j.addr.2017.12.010.

[12] L. Moreira, N.M. Guimarães, R.S. Santos, J.A. Loureiro, M.C. Pereira, N.F. Azevedo, Promising strategies employing nucleic acids as antimicrobial drugs, Mol. Therapy - Nucleic Acids 35 (2024) 102122, https://doi.org/10.1016/j.omtn.2024.102122.

[13] L. Popella, J. Jung, P.T. Do, R.J. Hayward, L. Barquist, J. Vogel, Comprehensive analysis of PNA-based antisense antibiotics targeting various essential genes in uropathogenic *Escherichia coli*, Nucleic Acids Res. 50 (2022) 6435–6452, https://doi.org/10.1093/nar/gkac362.

[14] L. Good, S.K. Awasthi, R. Dryselius, O. Larsson, P.E. Nielsen, Bactericidal antisense effects of peptide-PNA conjugates, Nat. Biotechnol. 19 (2001) 360–364, https://doi.org/10.1038/86753.

[15] N. Yavari, L. Goltermann, P.E. Nielsen, Uptake, stability, and activity of antisense anti-*acpP* PNA-peptide conjugates in *Escherichia coli* and the role of SbmA, ACS Chem. Biol. 16 (2021) 471–479, https://doi.org/10.1021/acschembio.0c00822.

[16] M. Pooga, T. Land, T. Bartfai, Ü. Langel, PNA oligomers as tools for specific modulation of gene expression, Biomol. Eng. 17 (2001) 183–192, https://doi.org/10.1016/S1389-0344(01)00075-2.

[17] C. Sharma, S.K. Awasthi, Versatility of peptide nucleic acids (PNAs): role in chemical biology, drug discovery, and origins of life, Chem. Biol. Drug Des. 89 (2017) 16–37, https://doi.org/10.1111/cbdd.12833.

[18] S. Kauppinen, B. Vester, J. Wengel, Locked nucleic acid (LNA): high affinity targeting of RNA for diagnostics and therapeutics, Drug Discov. Today Technol. 2 (2005) 287–290, https://doi.org/10.1016/j.ddtec.2005.08.012.

[19] A. Grünweiler, R.K. Hartmann, Locked nucleic acid oligonucleotides, BioDrugs 21 (2007) 235–243, https://doi.org/10.2165/00063030-200721040-00004.

[20] W.B. Wan, P.P. Seth, The medicinal chemistry of therapeutic oligonucleotides, J. Med. Chem. 59 (2016) 9645–9667, https://doi.org/10.1021/acs.jmedchem.6b00551.

[21] A.E. Paharik, H.L. Schreiber, C.N. Spaulding, K.W. Dodson, S.J. Hultgren, Narrowing the spectrum: the new frontier of precision antimicrobials, Genome Med. 9 (2017), https://doi.org/10.1186/s13073-017-0504-3.

[22] R.S. Santos, G.R. Dakwar, E. Zagato, T. Brans, C. Figueiredo, K. Raemdonck, N. F. Azevedo, S.C.D. Smedt, K. Braeckmans, Intracellular delivery of oligonucleotides in *helicobacter pylori* by fusogenic liposomes in the presence of gastric mucus, Biomaterials 138 (2017) 1–12, https://doi.org/10.1016/j.biomaterials.2017.05.029.

[23] L. Moreira, N.M. Guimarães, S. Pereira, R.S. Santos, J.A. Loureiro, R.M. Ferreira, C. Figueiredo, M.C. Pereira, N.F. Azevedo, Engineered liposomes to deliver nucleic acid mimics in *Escherichia coli*, J. Control. Release 355 (2023) 489–500, https://doi.org/10.1016/j.jconrel.2023.02.012.

[24] S. Pereira, R.S. Santos, L. Moreira, N. Guimarães, M. Gomes, H. Zhang, K. Remaut, K. Braeckmans, S.D. Smedt, N.F. Azevedo, Lipoplexes to deliver oligonucleotides in gram-positive and gram-negative bacteria: towards treatment of blood infections, Pharmaceutics 13 (2021) 989, https://doi.org/10.3390/pharmaceutics13070989.

[25] V. Percec, D.A. Wilson, P. Leowanawat, C.J. Wilson, A.D. Hughes, M.S. Kaucher, D. A. Hammer, D.H. Levine, A.J. Kim, F.S. Bates, K.P. Davis, T.P. Lodge, M.L. Klein, R. H. DeVane, E. Aqad, B.M. Rosen, A.O. Argintaru, M.J. Sienkowska, K. Rissanen, S. Nummelin, J. Ropponen, Self-assembly of janus dendrimers into uniform dendrimersomes and other complex architectures, Science 328 (2010) 1009–1014, https://doi.org/10.1126/science.1185547.

[26] Z. Lyu, L. Ding, A. Tintaru, L. Peng, Self-assembling supramolecular dendrimers for biomedical applications: lessons learned from poly(amidoamine) dendrimers, Acc. Chem. Res. 53 (2020) 2936–2949, https://doi.org/10.1021/acs.accounts.0c00589.

[27] F.S. Mehrabadi, W. Fischer, R. Haag, Dendritic and lipid-based carriers for gene/siRNA delivery (a review), Curr. Opinion Solid State Mater. Sci. 16 (2012) 310–322, https://doi.org/10.1016/j.cossms.2013.01.003.

[28] J. Chen, D. Zhu, X. Liu, L. Peng, Amphiphilic dendrimer vectors for RNA delivery: state-of-the-art and future perspective, Accoun. Mater. Res. 3 (2022) 484–497, https://doi.org/10.1021/accountsmr.1c00272.

[29] T. Wei, C. Chen, J. Liu, C. Liu, P. Posocco, X. Liu, Q. Cheng, S. Huo, Z. Liang, M. Fermeglia, S. Pricl, X.-J. Liang, P. Rocchi, L. Peng, Anticancer drug nanomicelles formed by self-assembling amphiphilic dendrimer to combat cancer drug resistance, Proc. Natl. Acad. Sci. 112 (2015) 2978–2983, https://doi.org/10.1073/pnas.1418494112.

[30] C. Chen, P. Posocco, X. Liu, Q. Cheng, E. Laurini, J. Zhou, C. Liu, Y. Wang, J. Tang, V.D. Col, T. Yu, S. Giorgio, M. Fermeglia, F. Qu, Z. Liang, J.J. Rossi, M. Liu, P. Rocchi, S. Pricl, L. Peng, Mastering dendrimer self-assembly for efficient siRNA delivery: from conceptual design to *in vivo* efficient gene silencing, Small 12 (2016) 3667–3676, https://doi.org/10.1002/smll.201503866.

[31] D. Dhumal, W. Lan, L. Ding, Y. Jiang, Z. Lyu, E. Laurini, D. Marson, A. Tintaru, N. Dusetti, S. Giorgio, J.L. Iovanna, S. Pricl, L. Peng, An ionizable supramolecular dendrimer nanosystem for effective siRNA delivery with a favorable safety profile, Nano Res. 14 (2021) 2247–2254, https://doi.org/10.1007/s12274-020-3216-8.

[32] D. Dhumal, B. Maron, E. Malach, Z. Lyu, L. Ding, D. Marson, E. Laurini, A. Tintaru, B. Ralahy, S. Giorgio, S. Pricl, Z. Hayouka, L. Peng, Dynamic self-assembling supramolecular dendrimer nanosystems as potent antibacterial candidates against drug-resistant bacteria and biofilms, Nanoscale 14 (2022) 9286–9296, https://doi.org/10.1039/D2NR02305A.

[33] T. Yu, X. Liu, A.-L. Bolcato-Bellemin, Y. Wang, C. Liu, P. Erbacher, F. Qu, P. Rocchi, J.-P. Behr, L. Peng, An amphiphilic dendrimer for effective delivery of small interfering RNA and gene silencing *in vitro* and *in vivo*, Angew. Chem. Int. Ed. 51 (2012) 8478–8484, https://doi.org/10.1002/anie.201203920.

[34] X. Liu, J. Zhou, T. Yu, C. Chen, Q. Cheng, K. Sengupta, Y. Huang, H. Li, C. Liu, Y. Wang, P. Posocco, M. Wang, Q. Cui, S. Giorgio, M. Fermeglia, F. Qu, S. Pricl, Y. Shi, Z. Liang, P. Rocchi, J.J. Rossi, L. Peng, Adaptive amphiphilic dendrimer-based nanoassemblies as robust and versatile siRNA delivery systems, Angew. Chem. Int. Ed. 53 (2014) 11822–11827, https://doi.org/10.1002/anie.201406764.

[35] X. Liu, C. Liu, J. Zhou, C. Chen, F. Qu, J.J. Rossi, P. Rocchi, L. Peng, Promoting siRNA delivery via enhanced cellular uptake using an arginine-decorated amphiphilic dendrimer, Nanoscale 7 (2015) 3867–3875, https://doi.org/10.1039/c4nr04759a.

[36] J. Chen, A. Ellert-Miklaszewska, S. Garofalo, A.K. Dey, J. Tang, Y. Jiang, F. Clément, P.N. Marche, X. Liu, B. Kaminska, A. Santoni, C. Limatola, J.J. Rossi, J. Zhou, L. Peng, Synthesis and use of an amphiphilic dendrimer for siRNA delivery into primary immune cells, Nat. Protoc. 16 (2020) 327–351, https://doi.org/10.1038/s41596-020-00418-9.

[37] J. Chen, D. Zhu, B. Lian, K. Shi, P. Chen, Y. Li, W. Lin, L. Ding, Q. Long, Y. Wang, E. Laurini, W. Lan, Y. Li, A. Tintaru, C. Ju, C. Zhang, S. Pricl, J. Iovanna, X. Liu, L. Peng, Cargo-selective and adaptive delivery of nucleic acid therapeutics by bola-amphiphilic dendrimers, Proc. Natl. Acad. Sci. 120 (2023) e2220787120, https://doi.org/10.1073/pnas.2220787120.

[38] Y. Jiang, Z. Lyu, B. Ralahy, J. Liu, T. Roussel, L. Ding, J. Tang, A. Kosta, S. Giorgio, R. Tomasini, X.-J. Liang, N. Dusetti, J. Iovanna, L. Peng, Dendrimer nanosystems for adaptive tumor-assisted drug delivery via extracellular vesicle hijacking, Proc. Natl. Acad. Sci. 120 (2023) e2215308120, https://doi.org/10.1073/pnas.2215308120.

[39] J. Liu, C. Chen, T. Wei, O. Gayet, C. Loncle, L. Borge, N. Dusetti, X. Ma, D. Marson, E. Laurini, S. Pricl, Z. Gu, J. Iovanna, L. Peng, X.-J. Liang, Dendrimeric nanosystem consistently circumvents heterogeneous drug response and resistance in pancreatic cancer, Exploration 1 (2021) 21–34, https://doi.org/10.1002/EXP.20210003.

[40] P. Garrigue, J. Tang, L. Ding, A. Bouhlel, A. Tintaru, E. Laurini, Y. Huang, Z. Lyu, M. Zhang, S. Fernandez, L. Balasse, W. Lan, E. Mas, D. Marson, Y. Weng, X. Liu, S. Giorgio, J. Iovanna, S. Pricl, B. Guillet, L. Peng, Self-assembling supramolecular dendrimer nanosystem for PET imaging of tumors, Proc. Natl. Acad. Sci. 115 (2018) 11454–11459, https://doi.org/10.1073/pnas.1812938115.

[41] L. Ding, Z. Lyu, A. Tintaru, E. Laurini, D. Marson, B. Louis, A. Bouhlel, L. Balasse, S. Fernandez, P. Garrigue, E. Mas, S. Giorgio, S. Pricl, B. Guillet, L. Peng, A self-assembling amphiphilic dendrimer nanotracer for SPECT imaging, Chem. Commun. 56 (2020) 301–304, https://doi.org/10.1039/c9cc07750b.

[42] L. Ding, Z. Lyu, T.-A. Perles-Barbacaru, A.Y.-T. Huang, B. Lian, Y. Jiang, T. Roussel, C. Galanakou, S. Giorgio, C.-L. Kao, X. Liu, J. Iovanna, M. Bernard, A. Viola, L. Peng, Modular self-assembling dendrimer nanosystems for magnetic resonance and multimodality imaging of tumors, Adv. Mater. 36 (2024) 2308262, https://doi.org/10.1002/adma.202308262.

[43] Z. Lyu, B. Ralahy, T.-A. Perles-Barbacaru, L. Ding, Y. Jiang, B. Lian, T. Roussel, X. Liu, C. Galanakou, E. Laurini, A. Tintaru, S. Giorgio, S. Pricl, X. Liu, M. Bernard, J. Iovanna, A. Viola, L. Peng, Self-assembling dendrimer nanosystems for specific fluorine magnetic resonance imaging and effective theranostic treatment of tumors, Proc. Natl. Acad. Sci. 121 (2024) e2322403121, https://doi.org/10.1073/pnas.2322403121.

[44] N. Zhang, D. Dhumal, S.H. Kuo, S.Q. Lew, P.D. Patil, R. Taher, S. Vaidya, C. Galanakou, A. Elkihel, M.W. Oh, S.Y. Chong, D. Marson, J. Zheng, O. Rouvinski, W.O. Abolarin, S. Pricl, G.W. Lau, L.T.O. Lee, L. Peng, Targeting the phosphatidylglycerol lipid: an amphiphilic dendrimer as a promising antibacterial candidate, Sci. Adv. 10 (2024) eadn8117, https://doi.org/10.1126/sciadv.adn8117.

[45] N. King, D. Dhumal, S.Q. Lew, S.H. Kuo, C. Galanakou, M.W. Oh, S.Y. Chong, N. Zhang, L.T.O. Lee, Z. Hayouka, L. Peng, G.W. Lau, Amphiphilic dendrimer as potent antibacterial against drug-resistant bacteria in mouse models of human infectious diseases, ACS Infect. Diseases 10 (2024) 453–466, https://doi.org/10.1021/acsinfecdis.3c00425.

[46] R.S. Santos, N. Guimarães, P. Madureira, N.F. Azevedo, Optimization of a peptide nucleic acid fluorescence in situ hybridization (PNA-FISH) method for the detection of bacteria and disclosure of a formamide effect, J. Biotechnol. 187 (2014) 16–24, https://doi.org/10.1016/j.jbiotec.2014.06.023.

[47] L. Moreira, N.M. Guimarães, S. Pereira, R.S. Santos, J.A. Loureiro, M.C. Pereira, N. F. Azevedo, Liposome delivery of nucleic acids in bacteria: toward *in vivo* labeling of human microbiota, ACS Infect. Diseases 8 (2022) 1218–1230, https://doi.org/10.1021/acsinfecdis.1c00601.

[48] C. Galanakou, D. Dhumal, L. Peng, Amphiphilic dendrimers against antibiotic resistance: light at the end of the tunnel? Biomater. Sci. 11 (2023) 3379–3393, https://doi.org/10.1039/D2BM01878K.

[49] Y. Zhang, W. Chen, D. Wu, Y. Liu, Z. Wu, J. Li, S.-Y. Zhang, Q. Ji, Molecular basis for cell-wall recycling regulation by transcriptional repressor MurR in *Escherichia coli*, Nucleic Acids Res. 50 (2022) 5948–5960, https://doi.org/10.1093/nar/gkac442.

[50] A. Vigouroux, B. Cordier, A. Aristov, L. Alvarez, G. Özbaykal, T. Chaze, E. R. Oldewurtel, M. Matondo, F. Cava, D. Bikard, S. van Teeffelen, Class-A penicillin binding proteins do not contribute to cell shape but repair cell-wall defects, eLife 9 (2020), https://doi.org/10.7554/elife.51998.

[51] D.A. Dik, D.R. Marous, J.F. Fisher, S. Mobashery, Lytic transglycosylases: concinnity in concision of the bacterial cell wall, Crit. Rev. Biochem. Mol. Biol. 52 (2017) 503–542, https://doi.org/10.1080/10409238.2017.1337705.

[52] E.A. Mueller, A.J. Egan, E. Breukink, W. Vollmer, P.A. Levin, Plasticity of *Escherichia coli* cell wall metabolism promotes fitness and antibiotic resistance across environmental conditions, eLife 8 (2019), https://doi.org/10.7554/elife.40754.

[53] D. Claessen, J. Errington, Cell wall deficiency as a coping strategy for stress, Trends Microbiol. 27 (2019) 1025–1033, https://doi.org/10.1016/j.tim.2019.07.008.

[54] J.J. Lazenby, E.S. Li, C.B. Whitchurch, Cell wall deficiency – an alternate bacterial lifestyle? Microbiology 168 (2022) https://doi.org/10.1099/mic.0.001218.

[55] A.K. Daitch, E.D. Goley, Uncovering unappreciated activities and niche functions of bacterial cell wall enzymes, Curr. Biol. 30 (2020) R1170–R1175, https://doi.org/10.1016/j.cub.2020.07.004.

[56] Y. Himeoka, N. Mitarai, Emergence of growth and dormancy from a kinetic model of the *Escherichia coli* central carbon metabolism, Phys. Rev. Re. 4 (2022), https://doi.org/10.1103/physrevresearch.4.043223.

[57] L.B. Thorfinnsdottir, G.H. Bø, J.A. Booth, P. Bruheim, Survival of escherichia coli after high-antibiotic stress is dependent on both the pregrown physiological state and incubation conditions, Front. Microbiol. 14 (2023), https://doi.org/10.3389/fmicb.2023.1149978.

[58] M. Rosenberg, N.F. Azevedo, A. Ivask, Propidium iodide staining underestimates viability of adherent bacterial cells, Sci. Rep. 9 (2019) 6483, https://doi.org/10.1038/s41598-019-42906-3.

[59] E.M.J. Vaessen, R.A.H. Timmermans, M.H. Tempelaars, M.A.I. Schutyser, H.M. W. den Besten, Reversibility of membrane permeabilization upon pulsed electric field treatment in *lactobacillus plantarum* WCFS1, Sci. Rep. 9 (2019) 19990, https://doi.org/10.1038/s41598-019-56299-w.

[60] P.R.G. Schindler, M. Teuber, Action of polymyxin B on bacterial membranes: morphological changes in the cytoplasm and in the outer membrane of *salmonella typhimurium* and *Escherichia coli* B, Antimicrob. Agents Chemother. 8 (1975) 95–104, https://doi.org/10.1128/AAC.8.1.95.

[61] C.J. Slingerland, I. Kotsogianni, C.M.J. Wesseling, N.I. Martin, Polymyxin stereochemistry and its role in antibacterial activity and outer membrane disruption, ACS Infect. Diseases 8 (2022) 2396–2404, https://doi.org/10.1021/acsinfecdis.2c00307.

[62] R. Rocha, C. Almeida, N.F. Azevedo, Influence of the fixation/permeabilization step on peptide nucleic acid fluorescence *in situ* hybridization (PNA-FISH) for the detection of bacteria, PLoS One 13 (2018) e0208867, https://doi.org/10.1371/journal.pone.0208867.

[63] U. Tsylents, I. Siekierska, J. Trylska, Peptide nucleic acid conjugates and their antimicrobial applications - a mini-review, Eur. Biophys. J. 52 (2023) 533–544, https://doi.org/10.1007/s00249-023-01673-w.

[64] J.N. Israelachvili, Van der Waals forces in biological systems, Q. Rev. Biophys. 6 (1973) 341–387, https://doi.org/10.1017/s0033583500001566.

[65] E.M. McCammick, V.S. Gomase, T.J. McGenity, D.J. Timson, J.E. Hallsworth, Water-hydrophobic compound interactions with the microbial cell, springer, Berlin Heidelberg (2010) 1451–1466, https://doi.org/10.1007/978-3-540-77587-4_99.

[66] T. Lu, Q. Chen, Van der Waals potential: an important complement to molecular electrostatic potential in studying intermolecular interactions, J. Mol. Model. 26 (2020), https://doi.org/10.1007/s00894-020-04577-0.

[67] T. Natsume, Y. Ishikawa, K. Dedachi, T. Tsukamoto, N. Kurita, Hybridization energies of double strands composed of DNA, RNA, PNA and LNA, Chem. Phys. Lett. 434 (2007) 133–138, https://doi.org/10.1016/j.cplett.2006.12.017.

[68] C. Briones, M. Moreno, Applications of peptide nucleic acids (PNAs) and locked nucleic acids (LNAs) in biosensor development, Anal. Bioanal. Chem. 402 (2012) 3071–3089, https://doi.org/10.1007/s00216-012-5742-z.

[69] C. Ghosh, L. Popella, V. Dhamodharan, J. Jung, J. Dietzsch, L. Barquist, C. Höbartner, J. Vogel, A comparative analysis of peptide-delivered antisense antibiotics employing diverse nucleotide mimics, RNA 30 (2024), https://doi.org/10.1261/rna.079969.124.

[70] C. Lou, S.V. Samuelsen, N.J. Christensen, B. Vester, J. Wengel, Oligonucleotides containing aminated 2′-amino-LNA nucleotides: synthesis and strong binding to complementary DNA and RNA, Bioconjug. Chem. 28 (2017) 1214–1220, https://doi.org/10.1021/acs.bioconjchem.7b00061.

[71] M.B. Danielsen, N.J. Christensen, P.T. Jørgensen, K.J. Jensen, J. Wengel, C. Lou, Polyamine-functionalized 2′-amino-LNA in oligonucleotides: facile synthesis of new monomers and high-affinity binding towards ssDNA and dsDNA, Chem. Eur. J. 27 (2021) 1416–1422, https://doi.org/10.1002/chem.202004495.

[72] R. Dryselius, S.K. Aswasti, G.K. Rajarao, P.E. Nielsen, L. Good, The translation start codon region is sensitive to antisense PNA inhibition in *Escherichia coli*, Oligonucleotides 13 (2003) 427–433, https://doi.org/10.1089/154545703322860753.

[73] J. Schindelin, I. Arganda-Carreras, E. Frise, V. Kaynig, M. Longair, T. Pietzsch, S. Preibisch, C. Rueden, S. Saalfeld, B. Schmid, J.Y. Tinevez, D.J. White,

V. Hartenstein, K. Eliceiri, P. Tomancak, A. Cardona, Fiji: an open-source platform for biological-image analysis, Nat. Methods 9 (2012) 676–682, https://doi.org/10.1038/nmeth.2019.
[74] Cytiva, PD SpinTrap™ G-25: Instructions for use, 2022.
[75] T.D. Minogue, H.A. Daligault, K.W. Davenport, K.A. Bishop-Lilly, S.M. Broomall, D. C. Bruce, P.S. Chain, O. Chertkov, S.R. Coyne, T. Freitas, K.G. Frey, H.S. Gibbons, J. Jaissle, C.L. Redden, C.N. Rosenzweig, Y. Xu, S.L. Johnson, Complete genome assembly of *Escherichia coli* ATCC 25922, a serotype O6 reference strain, Genome Announc. 2 (2014) 969–983, https://doi.org/10.1128/genomeA.00969-14.
[76] ATCC, *Escherichia coli* (Migula) Castellani and Chalmers - 25922, URL: https://www.atcc.org/products/25922, 2024.
[77] ATCC, *Bacillus subtilis* (Ehrenberg) Cohn - 6051, URL: https://www.atcc.org/products/6051, 2024.
[78] ATCC, *Staphylococcus epidermidis* (Winslow and Winslow) Evans - 35984, URL: https://www.atcc.org/products/35984, 2024.
[79] M. Motyl, K. Dorso, J. Barrett, R. Giacobbe, Basic microbiological techniques used in antibacterial drug discovery, Curr. Protoc. Pharmacol. 31 (2005) 1–22, https://doi.org/10.1002/0471141755.ph13a03s31.
[80] I. Wiegand, K. Hilpert, R.E.W. Hancock, Agar and broth dilution methods to determine the minimal inhibitory concentration (MIC) of antimicrobial substances, Nat. Protoc. 3 (2008) 163–175, https://doi.org/10.1038/nprot.2007.521.
[81] C.R. Mahon, D.C. Lehman, Textbook of Diagnostic Microbiology, 6 ed., Elsevier, 2018.
[82] Clinical and Laboratory Standards Institute (CLSI), Performance Standards for Antimicrobial Susceptibility Testing, 27 ed., 2017.
[83] B.D. Jett, K.L. Hatter, M.M. Huycke, M.S. Gilmore, Simplified agar plate method for quantifying viable bacteria, BioTechniques 23 (2018) 648–650, https://doi.org/10.2144/97234BM22.
[84] Molecular Probes Inc., Propidium iodide nucleic acid stain, URL: https://assets.thermofisher.com/TFS-Assets%2FLSG%2Fmanuals%2Fmp01304.pdf, 2006.
[85] A.S. Azevedo, C. Almeida, B. Pereira, P. Madureira, J. Wengel, N.F. Azevedo, Detection and discrimination of biofilm populations using locked nucleic acid/2'-O-methyl-RNA fluorescence *in situ* hybridization (LNA/2'OMe-FISH), Biochem. Eng. J. 104 (2015) 64–73, https://doi.org/10.1016/j.bej.2015.04.024.
[86] R.S. Santos, G.R. Dakwar, R. Xiong, K. Forier, K. Remaut, S. Stremersch, N. Guimarães, S. Fontenete, J. Wengel, M. Leite, C. Figueiredo, S.C.D. Smedt, K. Braeckmans, N.F. Azevedo, Effect of native gastric mucus on *in vivo* hybridization therapies directed at *helicobacter pylori*, Mol. Therapy - Nucleic Acids 4 (2015) e269, https://doi.org/10.1038/mtna.2015.46.
[87] D. Araújo, D. Mil-Homens, M. Henriques, S. Silva, Anti-EFG1 2'-OMethylRNA oligomer inhibits *Candida albicans* filamentation and attenuates the candidiasis in *galleria mellonella*, Mol. Therapy - Nucleic Acids 27 (2022) 517–523, https://doi.org/10.1016/j.omtn.2021.12.018.
[88] J.M. Loh, N. Adenwalla, S. Wiles, T. Proft, *Galleria mellonella* larvae as an infection model for group a streptococcus, Virulence 4 (2013) 419–428, https://doi.org/10.4161/viru.24930.
[89] C.J.Y. Tsai, J.M.S. Loh, T. Proft, *Galleria mellonella* infection models for the study of bacterial diseases and for antimicrobial drug testing, Virulence 7 (2016) 214–229, https://doi.org/10.1080/21505594.2015.1135289.